UNEP

AMAP

Global Mercury Modelling: Update of Modelling Results in the Global Mercury Assessment 2013

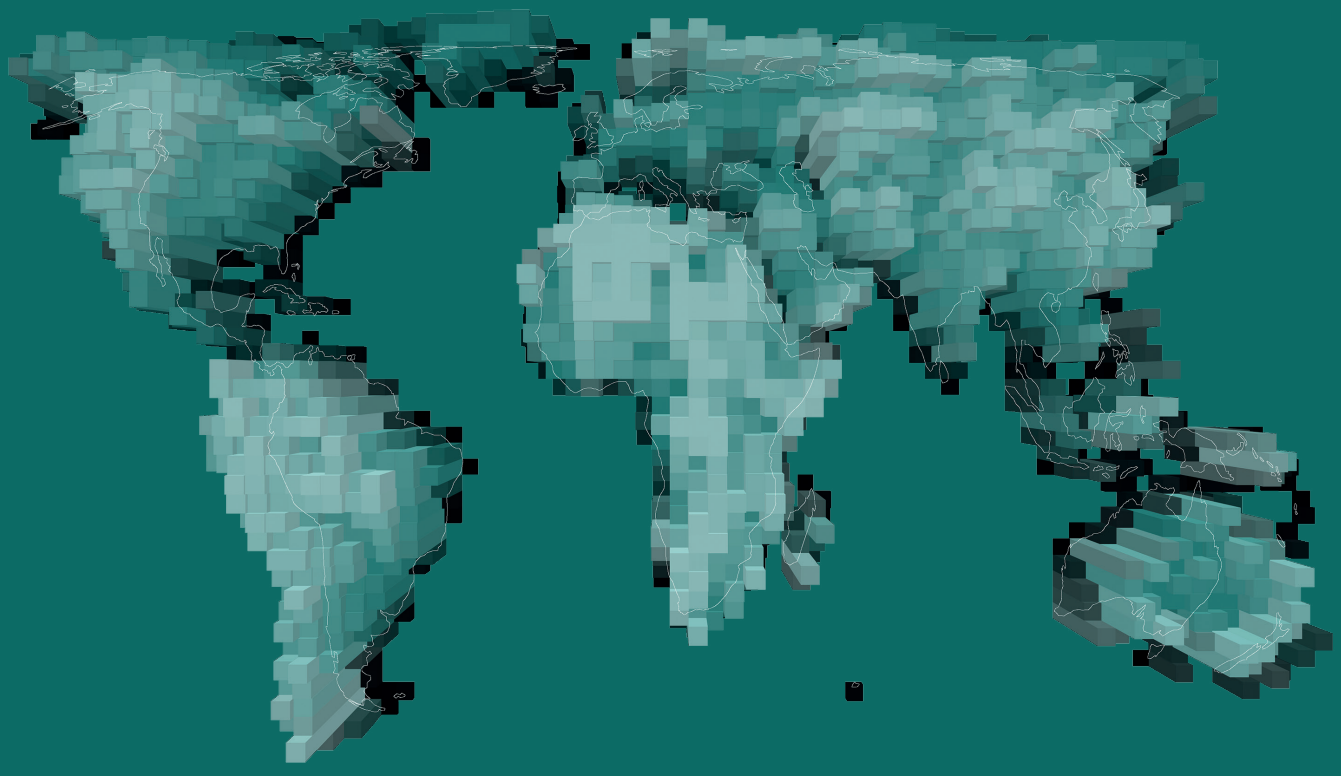

MSC-E

МСЦ-В

Authors and contributing experts

Oleg Travnikov *Meteorological Synthesizing Centre – East*
Ashu Dastoor *Environment Canada*
Carey Friedman *Massachusetts Institute of Technology*
Andrew Ryzhkov *Environment Canada*
Noelle Selin *Massachusetts Institute of Technology*
Shaojie Song *Massachusetts Institute of Technology*

Copyright:
© *Arctic Monitoring and Assessment Programme, 2015*

Citation: AMAP/UNEP, 2015. Global Mercury Modelling: Update of Modelling Results in the Global Mercury Assessment 2013. Arctic Monitoring and Assessment Programme, Oslo, Norway/UNEP Chemicals Branch, Geneva, Switzerland. iv + 32 pp.

The report can be found on the AMAP website *http://www.amap.no* and UNEP Chemicals Branch's website: *http://unep.org/chemicalsandwaste/*

AMAP/UNEP promote environmentally sound practices globally and in their own activities. This publication is printed on paper from environmentally-managed forests, using vegetable-based inks and other eco-friendly practices. Our distribution policy aims to reduce AMAP/UNEP's carbon footprint.

Production management
Simon Wilson, AMAP
Gunnar Futsæter, UNEP

Scientific, technical and linguistical editing
Carolyn Symon (carolyn.symon@btinternet.com)

Lay-out, graphics and technical production
Hugo Ahlenius, Nordpil *http://nordpil.com*

Printing
Narayana Press, Gylling, DK-8300 Odder, Denmark
http://www.narayanapress.dk
a swan-labelled printing company, 541 562

Cover photo:
Mercury vaporization and silver fusion stove in a Mexican silver mine. By unidentified author, published on Magasin Pittoresque, Paris, 1844 *http://www.shutterstock.com*

Disclaimer
The designations employed and the presentation of the material in this publication do not imply the expression of any opinion whatsoever on the part of the United Nations Environment Programme concerning the legal status of any country, territory, city or area or of its authorities, or concerning delimitation of its frontiers or boundaries. Moreover, the views expressed do not necessarily represent the decision or the stated policy of the United Nations Environment Programme, nor does citing of trade names or commercial processes constitute endorsement.

Reproduction
This publication may be reproduced in whole or in part and in any form for educational or non-profit purposes without special permission from the copyright holder, provided acknowledgement of the source is made. Material in this report can be freely quoted or reprinted. AMAP and UNEP would appreciate receiving a copy of any publication that uses this report as a source.

No use of this publication may be made for resale or for any other commercial purpose whatsoever without prior permission in writing from the Arctic Monitoring and Assessment Programme. AMAP grants UNEP full copyright permissions to this publication.

Produced by
Arctic Monitoring and Assessment Programme
AMAP Secretariat
Gaustadalléen 21
N-0349 Oslo
Norway

Tel. +47 21 08 04 80
Fax +47 21 08 04 85
amap@amap.no
http://amap.no

and

United Nations Environment Programme (UNEP)
Division of Technology, Industry and Economics (DTIE)
Chemicals Branch
International Environment House
11-13, Chemin des Anémones
CH-1219 Châtelaine (Geneva)
Switzerland

Tel. +41 (0) 22 917 81 92
Fax +41 (0) 22 797 34 60
metals.chemicals@unep.org
http://unep.org/chemicalsandwaste/

Contents

Acronyms

AMDE	Atmospheric Mercury Depletion Event
ASGM	Artisanal and small-scale gold mining
CIS countries	Countries of the Commonwealth of Independent States
FAO	UN Food and Agriculture Organization
GEM	Gaseous elemental mercury
GEOS-Chem	Chemical transport model, Massachusetts Institute of Technology
GLEMOS	Chemical transport model, Meteorological Synthesizing Centre - East
GMA 2013	Global Mercury Assessment 2013
GMHG	Chemical transport model, Environment Canada
GOM	Gaseous oxidized mercury
PBM	Particle bound mercury

1. Introduction

The Global Mercury Assessment 2013 (GMA 2013) (AMAP/UNEP, 2013) was prepared in accordance with the request of the UNEP's Governing Council (Decision 25/5 III, paragraph 36) to support negotiations on the development of the Minamata Convention on Mercury, a global treaty to reduce mercury pollution adopted by governments in October 2013. GMA 2013 covered a variety of aspects of the fate and transport of mercury in the environment including emissions to air and releases to the aquatic environment, dispersion and chemical transformations in the atmosphere and aquatic environment, and exchange fluxes between different environmental media. The assessment paid particular attention to the development of an up-to-date global inventory of anthropogenic mercury emissions. Evaluation of mercury pollution on a global scale was based on the analysis of available observational data and modelling results.

The current report aims to update the information presented in section 3.6 of the Technical Background Report for the Global Mercury Assessment 2013 (AMAP/UNEP, 2013) with new model simulation results and focusing on an evaluation of mercury intercontinental transport and source attribution of mercury deposition. The character of mercury dispersion in the atmosphere and transport from one region to another is largely affected by the physicochemical properties of the atmospheric mercury species. Poorly soluble and relatively stable gaseous elemental mercury (GEM) can drift in the air for months providing transport of mercury mass between different regions of the planet. In contrast, oxidized mercury species – gaseous oxidized mercury (GOM) and particle bound mercury (PBM) – are easily removed from the air by precipitation scavenging or surface uptake (Selin, 2009; Travnikov, 2011; AMAP/UNEP, 2013). Therefore, levels of mercury deposition and its source apportionment in each region are determined by the magnitude and speciation of domestic emissions, emissions in other regions and by the oxidative capacity of the atmosphere that transforms globally dispersed GEM to deposited GOM and PBM. As has been shown in previous studies (Seigneur et al., 2004; Selin et al., 2008; Travnikov and Ilyin, 2009; Corbitt et al., 2011; Lei et al., 2013; Chen et al., 2014), atmospheric transport from distant sources can make a significant contribution to mercury deposition, particularly in regions with low domestic emissions. On the other hand, the proportion of anthropogenic emissions that deposit locally or regionally depends on emissions speciation, which differs significantly for different emission sectors. Besides, the impact of long-range transport on mercury deposition can vary seasonally due to change in air concentrations of mercury oxidizing agents that lead to change in GEM oxidation intensity and subsequent deposition.

The current study is based on multi-model simulations of mercury atmospheric transport performed as part of the Mercury Modelling Task Force (MMTF), a scientific cooperative initiative under the Global Mercury Observation System (GMOS, www.gmos.eu), aimed at improving current understanding of the key mercury atmospheric processes and evaluating present and future levels of mercury pollution. Simulation results of the multi-model ensemble (see Annex A) are used to quantify global patterns of mercury air concentration and deposition (Chapter 2), source apportionment of mercury deposition to major geographical regions and aquatic areas of the global ocean as well as seasonal variation in source-receptor relationships (Chapter 3), and deposition from different emission sectors (Chapter 4). Simulation results for each individual model of the ensemble are presented in Annex B.

2. Global patterns of mercury air concentration and deposition

An ensemble of three chemical transport models (GLEMOS, GEOS-Chem, GMHG) was applied for evaluating atmospheric mercury dispersion and deposition on a global scale in 2013. A brief summary of the main features of the participating models is given in Annex A. The models also took part in the multi-model assessment of mercury pollution presented in GMA 2013 (AMAP/UNEP, 2013). The models differ significantly in their formulation including different horizontal and vertical resolution, and differences in their description of mercury atmospheric chemistry and their parameterization of specific processes (e.g. dry and wet deposition, atmospheric mercury depletion events – AMDEs – in the polar regions etc.). Two of the three models (GLEMOS and GMHG) are mainly atmospheric models simulating mercury transport in the atmosphere and exchange with the Earth's surface (deposition and re-emission), whereas the remaining model (GEOS-Chem) presents a full multi-media description of mercury cycling in the environment. The models also differ in their estimates of natural and legacy emissions of mercury to the atmosphere. Thus, the multi-model ensemble reflects the range of contemporary approaches applied for simulations of mercury contamination and partly characterizes uncertainties associated with gaps in knowledge on mercury processes in the environment.

The global inventory of mercury anthropogenic emissions for 2010 (AMAP/UNEP, 2013) was used in the present study. The dataset consists of gridded emission data with a spatial resolution of 0.5° × 0.5° for three mercury species (GEM, GOM, PBM). The total global emission of mercury from anthropogenic sources is estimated at 1875 t/y. This estimate of total emissions is somewhat lower than the total mercury emission reported in GMA 2013 (1960 t/y), because it does not include emissions from contaminated sites which were not spatially distributed (AMAP, 2014). The overall proportions of GEM, GOM, and PBM emissions are 81%, 15% and 4%, respectively. This is based on a simple emissions speciation scheme applied to the primary sector emissions estimates, which also assigned emissions to three classes of source

height: h ≤50 m, h = 50–150 m, h ≥ 150 m. It should be noted, however, that some models of the ensemble modified the original anthropogenic emissions speciation scheme mentioned above following the model formulation (Annex A, Table A-1). There is no information on temporal variation of emissions available in the dataset.

The spatial distribution of the total annual anthropogenic mercury emission over the globe in 2010 is illustrated in Figure 1a and the speciation of emissions in different geographical regions in Figure 1b (see Chapter 3 for a definition of the source regions). Significant mercury emissions are characteristic of industrial regions in East and South Asia, Central Europe and the eastern part of North America. These regions are also characterized by an increased share of oxidized mercury forms (GOM and PBM). In addition, high emission fluxes are typical for some areas of Central and South America, Sub-Saharan Africa and Southeast Asia due to mercury releases from artisanal and small-scale gold mining (ASGM), mostly as GEM. Almost no emissions are expected in the Arctic and Antarctic regions.

a)

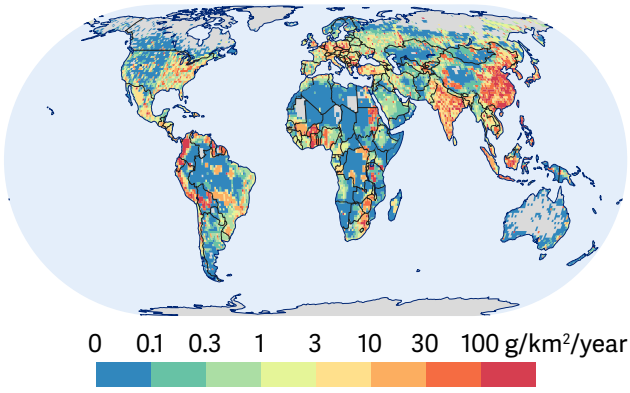

b)

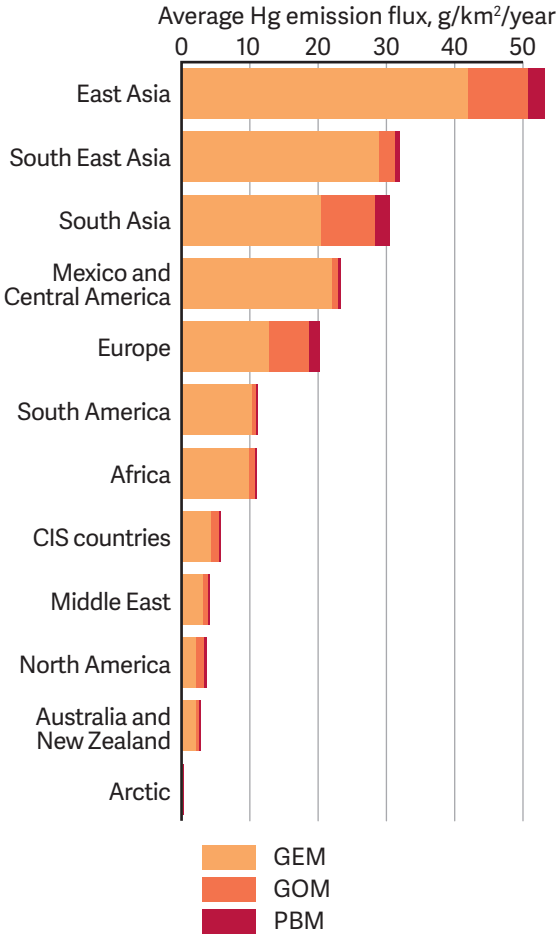

Figure 1. Global distribution of anthropogenic mercury emissions in 2010 (a) and speciation of mercury emissions for in different geographical regions (b)

The simulated spatial distribution of GEM in ambient air and total mercury deposition fluxes are shown in Figure 2. The concentration of GEM has a pronounced south-to-north gradient (Figure 2a). Mercury concentrations in the southern hemisphere are mostly below 1.2 ng/m^3, whereas concentrations in the northern hemisphere range between 1.3 and 1.4 ng/m^3 over the ocean and commonly exceed 1.4 ng/m^3 over land. GEM concentrations in East and South Asia are higher than those in Europe, which in turn are somewhat greater than those in North America. This pattern generally reflects the spatial distribution of anthropogenic mercury emissions (Figure 1a). Elevated concentrations simulated by the models in the northern part of South America and in Sub-Saharan Africa are caused by a large contribution of emissions from ASGM. .

The calculated global distribution of mercury deposition in 2013 is shown in Figure 2b. Along with high mercury deposition fluxes over large industrial regions (East and South Asia, Europe, North America etc.) and regions with significant mercury emissions from ASGM (Southeast Asia, Central and South America, Sub-Saharan Africa) relatively large deposition

a)

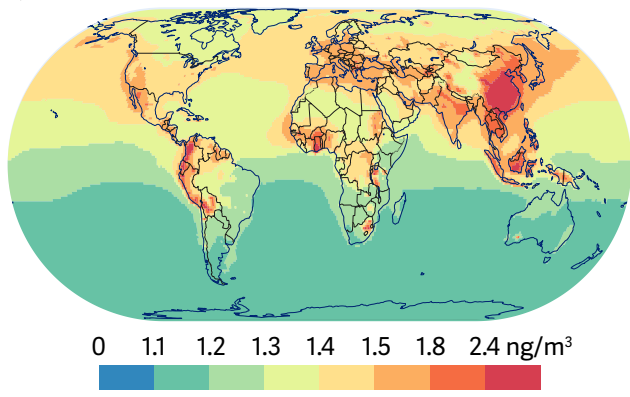

b)

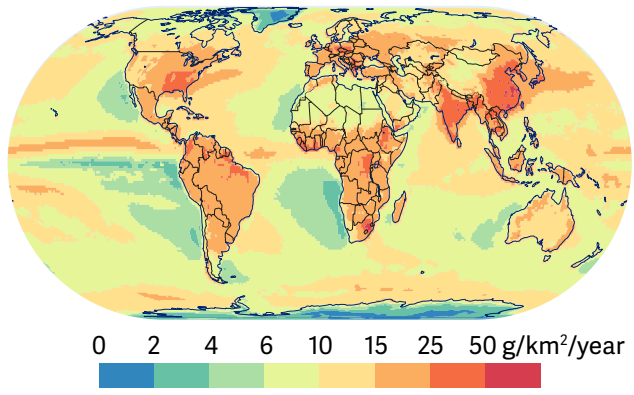

Figure 2. Global distribution of ensemble mean annual GEM concentration in ambient air (a) and annual total mercury deposition (b) in 2013.

is also detected over some remote areas of the oceans and in the polar regions. The former includes, for instance, elevated mercury deposition in the Intertropical Convergence Zone (ITCZ; a belt of converging trade winds and rising air that encircles the Earth near the equator) due to high precipitation intensity. The latter is characterized by intensive oxidation of GEM in the lower troposphere during AMDEs, leading to increased mercury deposition in spring.

Atmospheric deposition of mercury includes a significant contribution from natural and legacy sources. The relative contributions of contemporary anthropogenic emissions and natural/legacy emissions are shown in Figure 3. The graphic also includes average mercury deposition fluxes in various geographical regions. The relative contributions of the two source types are comparable in size only in three source regions – South Asia, East Asia and Europe. In the other regions the share of current anthropogenic sources varies between 20% and 35%. The contribution of natural/legacy sources is generally greater in remote regions with lower atmospheric deposition. It should be noted that the three models agree relatively well in their simulation of current anthropogenic deposition (see Annex B, Figure B-3). In contrast, estimates of mercury deposition from natural/legacy sources vary within a factor of 2 indicating higher uncertainty of the multi-model results for this deposition component.

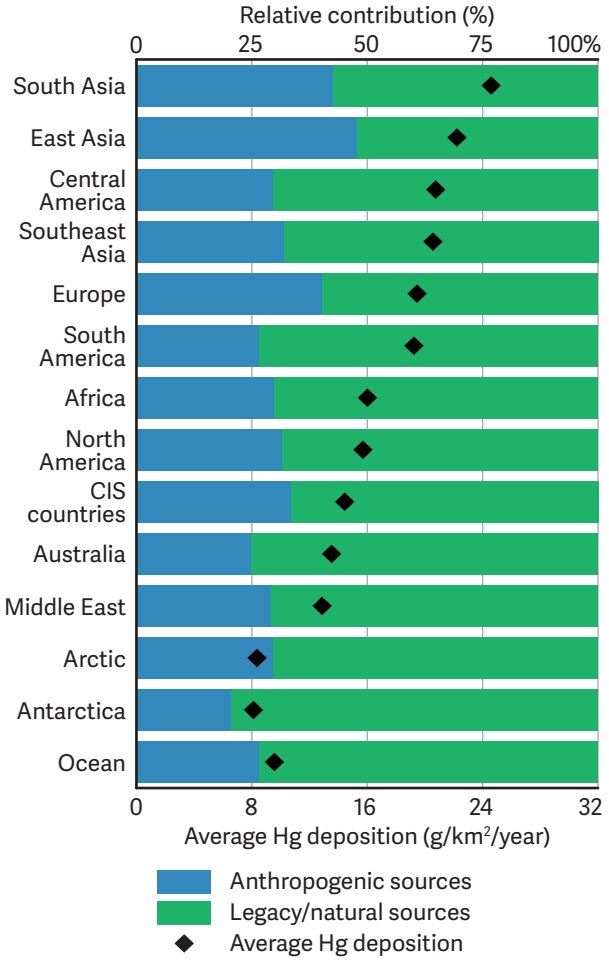

Figure 3. Average mercury deposition flux over various geographical regions in 2013 and the relative contribution of anthropogenic and natural/legacy source types to deposition as simulated by the chemical transport model ensemble.

The main pathway of human exposure to mercury is through fish consumption (Mahaffey et al., 2004, 2009; Sunderland et al., 2010). Mercury enters marine and freshwater ecosystems through direct anthropogenic releases, atmospheric deposition, riverine run-off and other pathways. In water bodies and bottom sediments inorganic mercury is converted by biotic and/or abiotic processes to methylmercury, a highly toxic organic form of mercury which accumulates and biomagnifies in aquatic food webs (Wiener et al., 2003; Sunderland et al., 2004, 2009, 2010; Cossa et al., 2009). It has been suggested that most methylmercury accumulating in ocean fish is derived from in situ methylmercury production within the upper waters, with the main source of mercury in the open ocean being atmospheric deposition (Mason et al., 2012). To estimate mercury loads to different aquatic regions and so connect these with potential accumulation in fish, mercury deposition has been calculated for the major fishing areas according to the classification of the UN Food and Agriculture Organization (FAO, 2014a). It should be noted that these rough estimates do not reflect the chain of processes leading to the accumulation of mercury in fish (aquatic chemistry, methylation, movement through the trophic web etc.) but rather indicate aquatic regions with the potential risk of fish contamination by mercury.

Figure 4a shows the spatial distribution of the ensemble mean annual mercury deposition over the ocean in 2013 in relation to the FAO Major Fishing Areas (specifications of the fishing

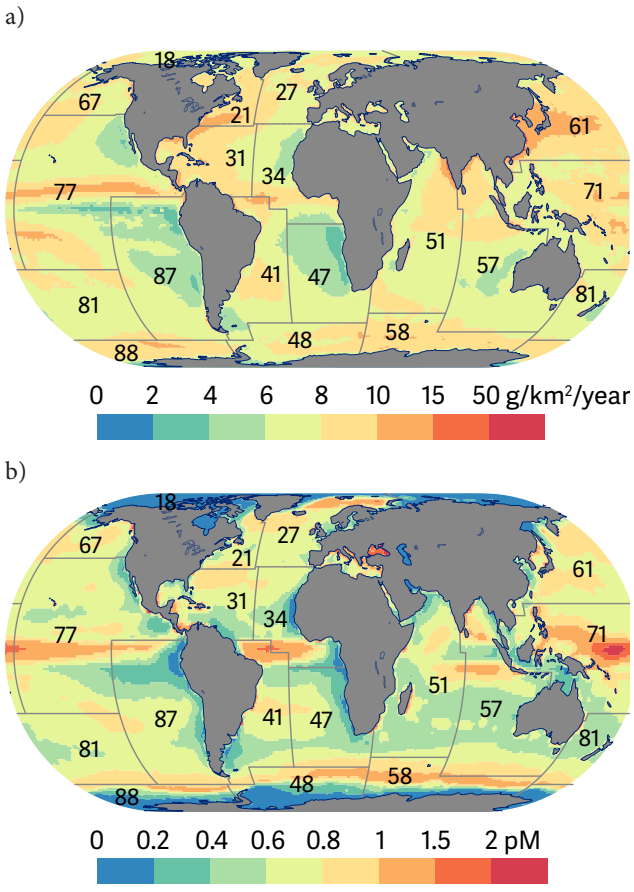

Figure 4. Spatial distribution of ensemble mean annual mercury deposition over the ocean in 2013 (a) and total mercury concentration in seawater simulated by GEOS-Chem (b). Lines show the FAO Major Fishing Areas (FAO, 2014a).

areas are given in Table 1). The global distribution of total mercury concentration in seawater simulated by one of the models (GEOS-Chem) is shown in Figure 4b. The highest deposition fluxes are over the Northwest Pacific (area 61), Northwest Atlantic (area 21), Western Central Atlantic (area 31) and Western Central Pacific (area 71). Significant fluxes are also detected over the Antarctic Indian Ocean (area 58) and Antarctic Pacific (area 88). The simulated pattern of mercury concentration in seawater generally follows the deposition distribution. The highest concentrations are characteristics of the equatorial parts of the Atlantic and Pacific Oceans, the Northeast Atlantic, and some areas of the Southern Ocean. High concentrations are also obtained for the Mediterranean and Black Sea.

Figure 5 shows annual mercury deposition and concentration in seawater averaged over the FAO Major Fishing Areas. The graphic also includes the total annual marine capture fisheries production according to FAO statistics for 2012 (FAO, 2014b). The largest total capture production takes place in the Northwest Pacific (area 61), Western Central Pacific (area 71) and Northeast Atlantic (area 27). These areas are also characterized by significant mercury deposition (10–15 g/km^2/y on average). The mercury concentration in some locations of these aquatic areas reaches maximum values (more than 1.5 pM). Total fisheries production is also significant in the Southeast Pacific (area 87) and the Eastern Indian Ocean (area 57), where atmospheric mercury deposition and seawater concentration are both relatively low.

Table 1. Specification of the FAO Major Fishing Areas (FAO, 2014a)

Fishing area	Code
Atlantic Ocean	
Northwest Atlantic	21
Northeast Atlantic	27
Western Central Atlantic	31
Eastern Central Atlantic	34
Southwest Atlantic	41
Southeast Atlantic	47
Arctic Sea	18
Mediterranean and Black Seas	37
Pacific Ocean	
Northwest Pacific	61
Northeast Pacific	67
Western Central Pacific	71
Eastern Central Pacific	77
Southwest Pacific	81
Southeast Pacific	87
Indian Ocean	
Western Indian Ocean	51
Eastern Indian Ocean	57
Southern Ocean	
Antarctic Atlantic	48
Antarctic Indian Ocean	58
Antarctic Pacific	88

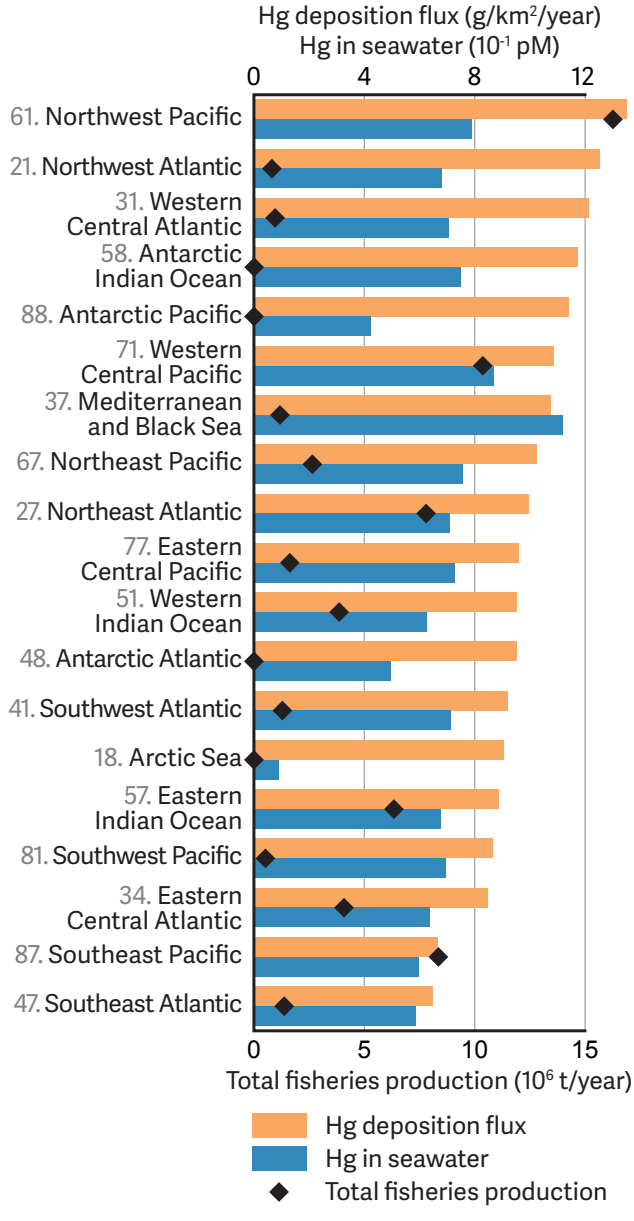

Figure 5. Average annual mercury deposition and total mercury concentration in the FAO Major Fishing Areas in 2013. Total annual marine capture fisheries production in 2012 is given for the same areas for comparison (FAO, 2014b).

3. Estimates of mercury intercontinental transport

Source apportionment of mercury deposition, illustrating atmospheric transport of mercury between different continents and regions, was evaluated by the three models. The definition of source and receptor regions adopted in the study is shown in Figure 6. The regions considered include the continents (Europe, North, Central and South America, Africa, Australia), large sub-continents (Middle East, countries of the Commonwealth of Independent States (CIS), South, East and Southeast Asia) and the Polar Regions (Figure 6a). The total anthropogenic emission of mercury from the selected geographical regions is shown in Figure 6b. The largest anthropogenic emissions are estimated for East Asia (616 t/y) and Africa (329 t/y). Considerable emissions (120–170 t/y) are also estimated for South America, Southeast and South Asia, and Central America. The smallest emissions are characteristics of Australia, Middle East and the Arctic (AMAP/UNEP, 2013).

As previously mentioned, mercury deposition in all regions consists of a contribution from contemporary anthropogenic emissions and a large contribution from natural/legacy sources. The former includes deposition from domestic emissions and mercury transported into the region from sources located in other regions. A comparison of the relative contributions of domestic and foreign anthropogenic sources to total mercury deposition in various regions as simulated by the model ensemble is illustrated in Figure 7. The share of domestic sources varies from zero in Antarctica to 36% in East Asia. In most regions (except for East Asia) the contribution of foreign sources is within the range 15–30%. In general, this agrees well with conclusions drawn in GMA 2013 (AMAP/UNEP 2013). In two regions (East and South Asia) the contribution of domestic sources (25–36%) exceeds the contribution of sources located outside the region (12–18%). This is due to significant anthropogenic emissions in these regions and to the dominant role played by emissions from industrial and combustion sources. Emissions from these sources contain an essential fraction of oxidized mercury, which mostly deposits within the region (Chapter). In Europe, both domestic and foreign emissions contribute almost equally (20%) to total mercury deposition. It should be noted that the models differ somewhat in their estimates of the relative contribution of domestic and foreign sources to average mercury deposition (Annex B, Figure B-4). The main reason for this is the difference in chemical speciation of anthropogenic emissions used by the models.

Some large contributors to global mercury emission – Africa, South America and Southeast Asia – are characterized by a considerably lower contribution of domestic sources (6–11%). This can be explained by the considerable portion of emissions from ASGM in these regions, which contain mercury in gaseous elemental form. The majority of these emissions contribute to global transport rather than deposition within the region. The lowest contributions of domestic sources were estimated for the Middle East (3%), Australia (2%) and the Arctic (1%), which are characterized by the lowest anthropogenic emissions

a)

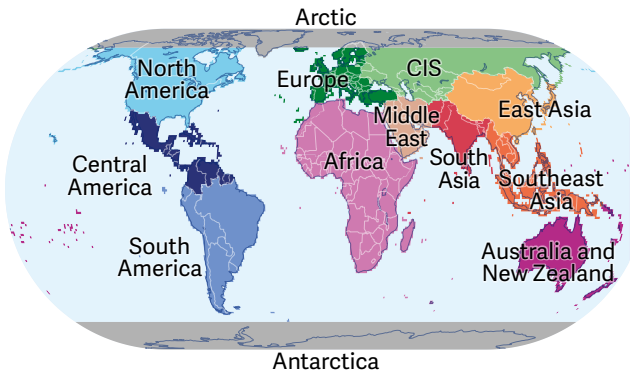

b)

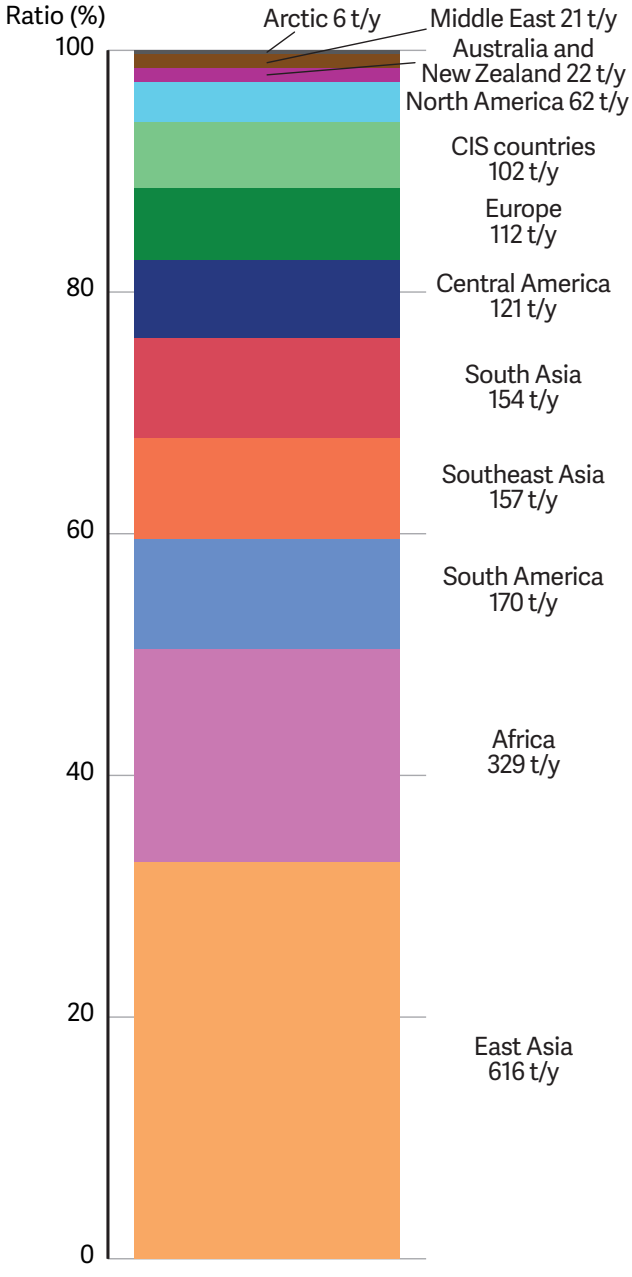

Figure 6. Definition of source and receptor regions used in the analysis (a) and the share of global anthropogenic mercury emissions among the source regions (b).

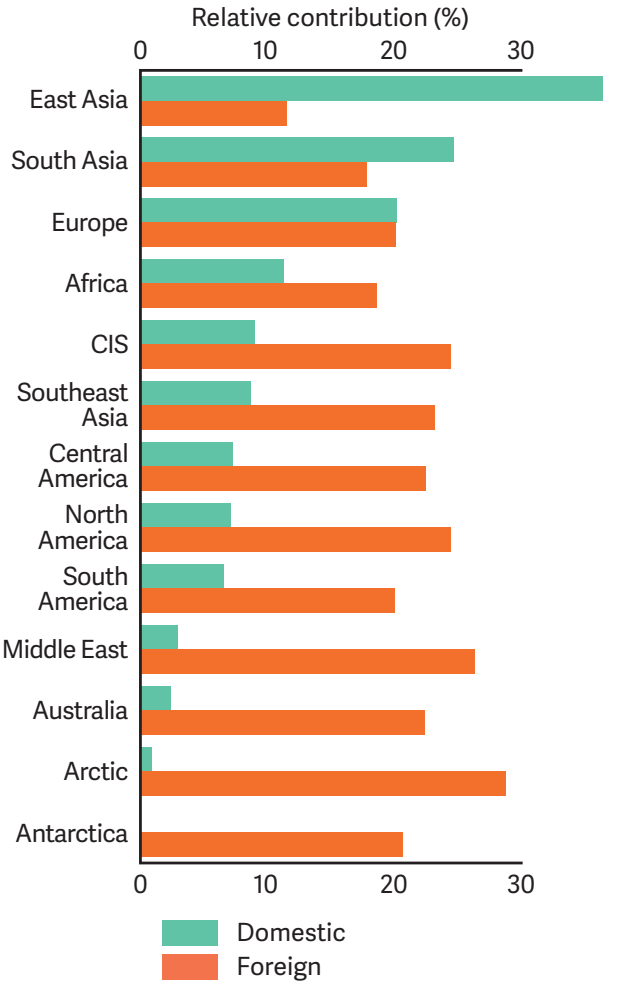

Figure 7. Relative contribution of domestic and foreign anthropogenic sources to total mercury deposition over various regions.

(Figure 6b). It should be noted that above average characteristics of mercury deposition can vary noticeably within the regions due to the uneven spatial distribution of emission sources. In particular, the contribution of domestic sources can be significantly higher in the vicinity of large point sources and industrial areas.

Figure 8 presents a source region apportionment of mercury deposition from contemporary anthropogenic sources to various geographical regions of the world. As previously mentioned, anthropogenic mercury deposition to Europe is derived almost equally from domestic and foreign emissions. The largest contributors to foreign emissions include East Asia (20%), Africa (8%), CIS countries (5%), and South Asia (3%). In North America the contribution of domestic sources (23%) is even smaller than the foreign contribution of East Asia (32%). Africa (12%), CIS countries (6%) and Central America (6%) are among other significant foreign contributors of deposition from contemporary anthropogenic emissions to North America. In contrast, anthropogenic mercury deposition to East and South Asia is dominated by contributions from domestic sources (76% and 58%, respectively). The major foreign contribution to these regions consists of the mutual transport between the regions and the considerable contribution from Africa. Mercury deposition to remote regions such as the Arctic and Antarctica is determined by long-range atmospheric transport from the

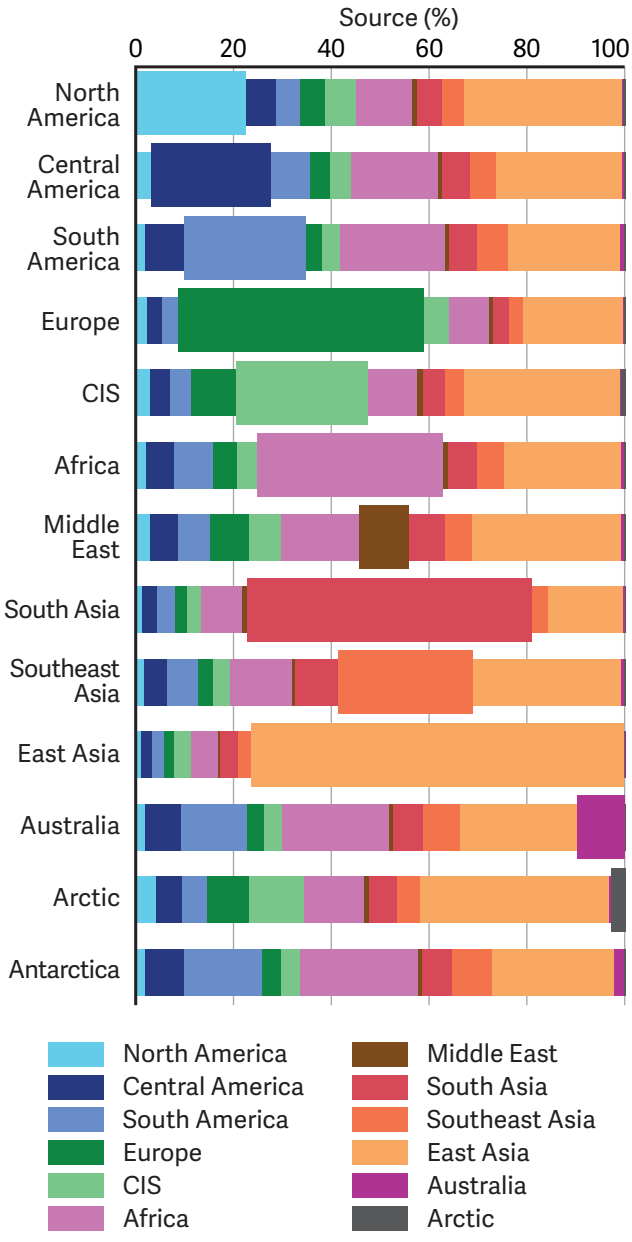

Figure 8. Source region apportionment of mercury deposition from contemporary anthropogenic emissions to various geographical regions in 2013.

major source regions. The main contributors for both regions are East Asia and Africa. The Arctic is also affected by emission sources in Europe and the CIS countries, and Antarctica by South and Central Americas.

Mercury deposition to aquatic regions is affected both by shoreline emission sources and by long-range atmospheric transport. Figure 9 shows East Asia to be the largest contributor to mercury deposition in almost all aquatic regions. Its contribution to mercury deposition from contemporary anthropogenic sources varies from 25% to 53%. It is followed by sources located in Africa (11–26%). The exception is the Mediterranean and Black Sea region, which is dominated by European emissions. As previously mentioned, the regions where considerable mercury deposition is accompanied by

large total capture fisheries production include the Northwest Pacific, the Western Central Pacific and the Northeast Atlantic (Chapter 2). Anthropogenic mercury deposition in these regions is mostly determined by emissions from East Asia, Africa, Europe, CIS countries, South and Southeast Asia.

Both the absolute and relative contributions of different source regions to mercury deposition vary over the year. Figure 10 presents the model ensemble mean seasonal variation of source region apportionment of mercury deposition to the various geographical regions in 2013. Seasonal variation of deposition from domestic sources is considerably less than that from foreign and natural/legacy sources. Particularly in Europe, the CIS countries, North and Central Americas (Figs. 10a–d). It should be noted that temporal variation of direct anthropogenic emissions is not taken into account in the study. Given that local and regional mercury deposition is largely caused by removal of directly emitted oxidized mercury forms (GOM and PBM), variation of deposition from domestic sources is mostly determined by changes in the environmental conditions affecting removal processes (precipitation amount, stability of atmospheric boundary layer, vegetation height etc.).

In contrast, the deposition of mercury transported from other regions is highly affected by oxidation chemistry, which converts GEM transported in the atmosphere to GOM and PBM deposited to the ground by wet removal and surface uptake. Therefore, the contribution of foreign sources is greater in summer when mercury oxidation is more intensive. In the case of natural and legacy sources, the seasonal pattern is also affected by the intensity of mercury evasion from the surface. During the warm season, natural and legacy emission of mercury are greater due to higher temperatures and solar radiation as well as to the absence of snow cover. Seasonal variation of mercury deposition is also pronounced in southern hemisphere regions (South America and Australia) with maximum deposition in summer and minimum deposition in winter (Figs. 10g–h). Deposition in the Arctic and Antarctica has pronounced maximums in spring, due to intensive mercury oxidation and removal during AMDEs (Figs. 10i–j).

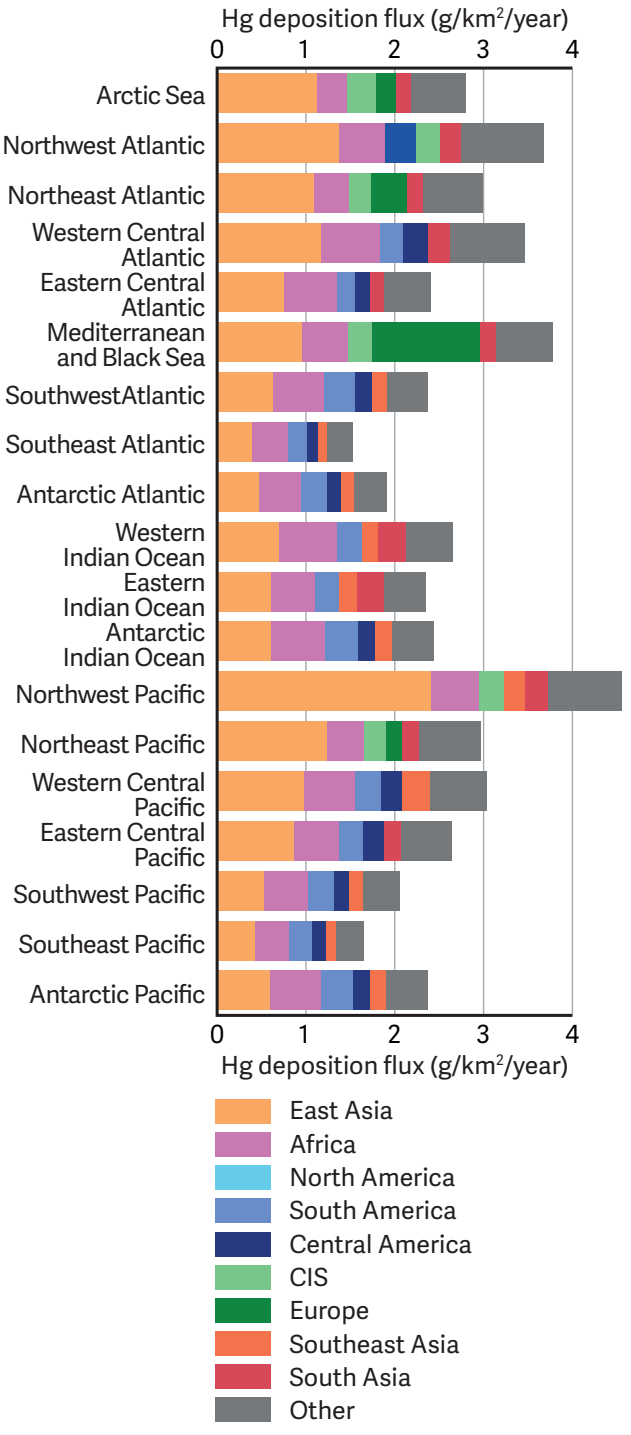

Figure 9. Source region apportionment of mercury deposition from contemporary anthropogenic sources to various aquatic regions in 2013

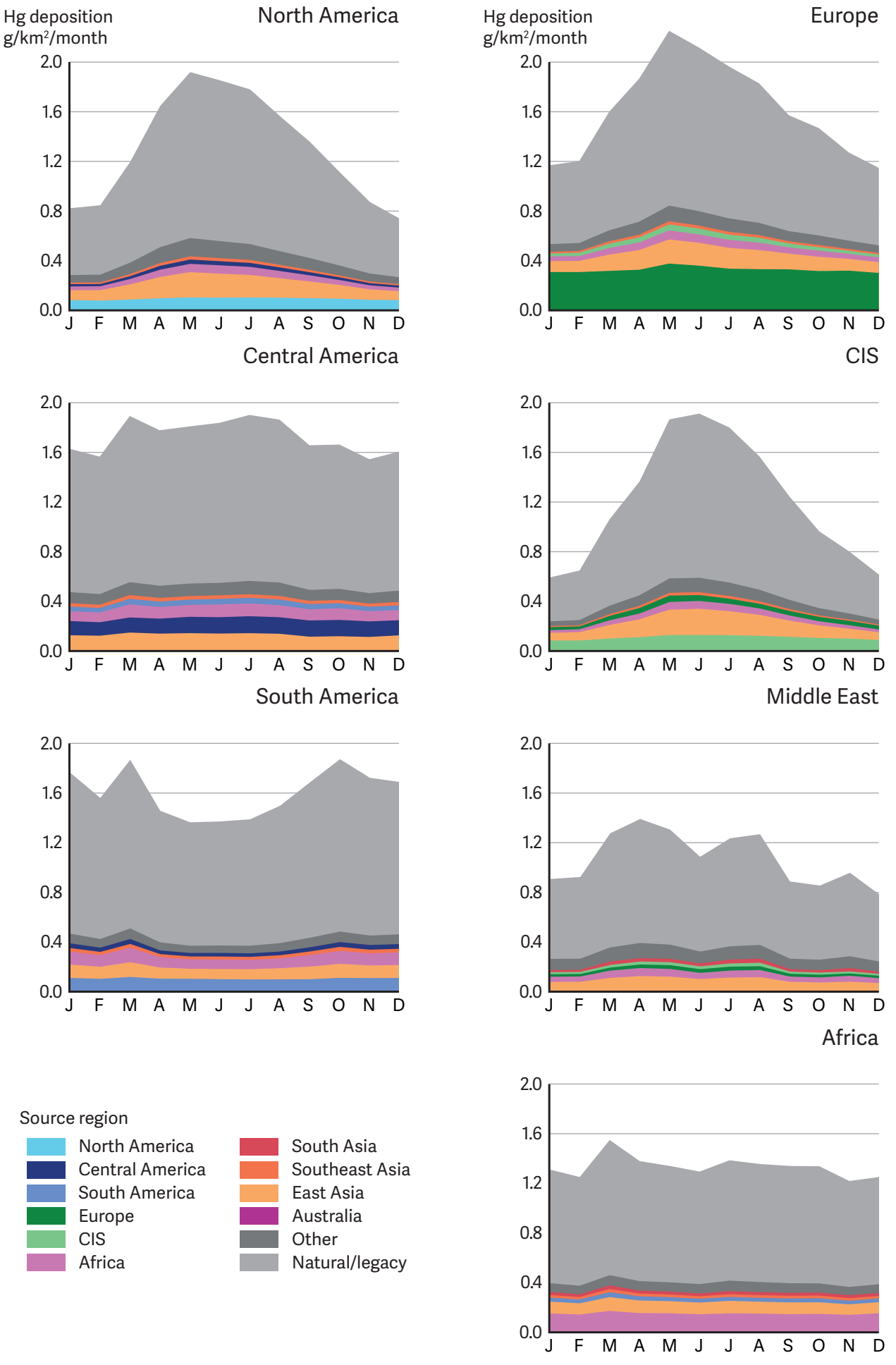
Hg deposition
g/km²/month
North America
Europe
Central America
CIS
South America
Middle East
Africa
2.0
1.6
1.2
0.8
0.4
0.0
J F M A M J J A S O N D
Source region
North America
Central America
South America
Europe
CIS
Africa
South Asia
Southeast Asia
East Asia
Australia
Other
Natural/legacy

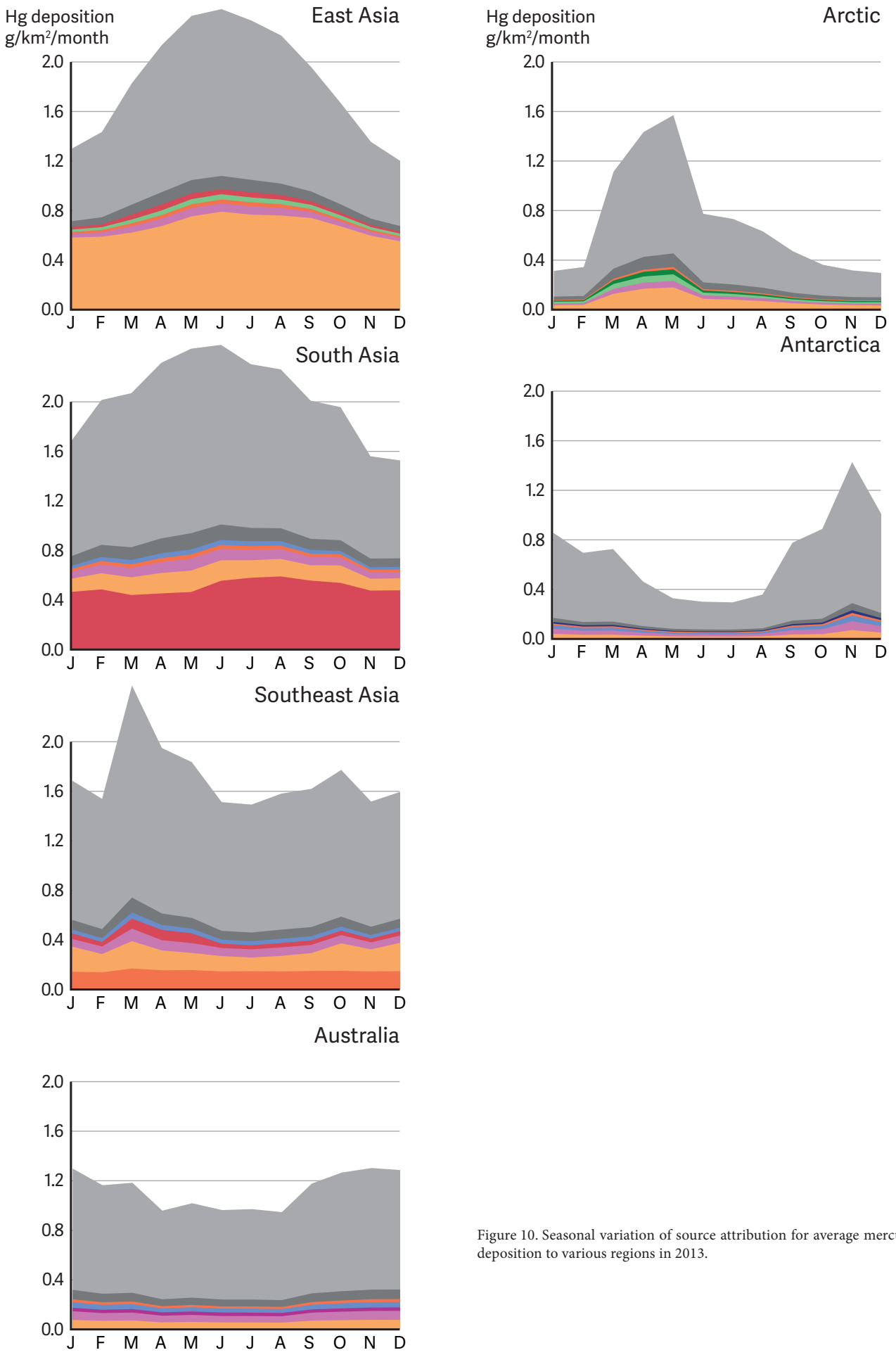

Figure 10. Seasonal variation of source attribution for average mercury deposition to various regions in 2013.

4. Mercury deposition from different emission sectors

The model ensemble was also applied for simulating mercury deposition from different anthropogenic emissions sectors. The sectors of mercury anthropogenic emissions were aggregated into three general groups in this subset: stationary combustion sources including power plants and distributed heating; industrial sources including stationary combustion for industry; intentional use and product waste associated sectors including ASGM.

A more detailed description of the emission sector groups is given in Table B-4 of Annex B. The spatial distribution of mercury emissions from the sector groups is shown in Figure 11. The majority of emissions from stationary combustion sources are located in the largest industrial and populated regions of the northern hemisphere – East and South Asia, Europe and North America – as well as in southern Africa in the southern hemisphere (Figure 11a). Emissions from industrial sources are more widely scattered than for stationary combustion sources (Figure 11b). South America, Sub-Saharan Africa and East and Southeast Asia are responsible for a significant proportion of mercury emissions from intentional use and product waste (Figure 11c). Total mercury emissions are 379, 642 and 854 t/y for stationary combustion, industrial sources and intentional use and product waste, respectively.

The chemical speciation of mercury emissions differs considerably between different sector groups (Figure 11d). According to the applied inventory (AMAP/UNEP, 2013; AMAP, 2014), emissions from stationary combustion consist of approximately equal contributions of elemental mercury (GEM) and oxidized forms (GOM, PBM). The proportion of oxidized mercury is much smaller in emissions from industrial sources (20%). More than 95% of mercury emissions from intentional use and product waste are in the elemental gaseous form. However, estimates of mercury emissions speciation are associated with significant uncertainties (Amos et al., 2012; Zhang et al., 2012; Kos et al., 2013) and this can affect the results of the analysis.

Simulated global patterns of the relative contributions of the three sector groups to total mercury deposition are shown in Figure 12. The impact of stationary combustion sources is mostly limited to the large industrial regions in East and South Asia, Europe, the eastern part of North America and South Africa, where the contribution of this sector group exceeds 20–30% of total mercury deposition (Figure 12a). In contrast, the contribution of stationary combustion sources is below 10% in other regions. The spatial difference is determined by the significant proportion of short-lived oxidized mercury forms in emissions from this sector group, and leads to strong mercury deposition in the vicinity of the source regions. Emissions from industrial sources affect the whole northern hemisphere, where the contribution to deposition of this sector group exceeds 10% (Figure 12b). Mercury released from intentional use and product waste (mostly as GEM) can be transported globally.

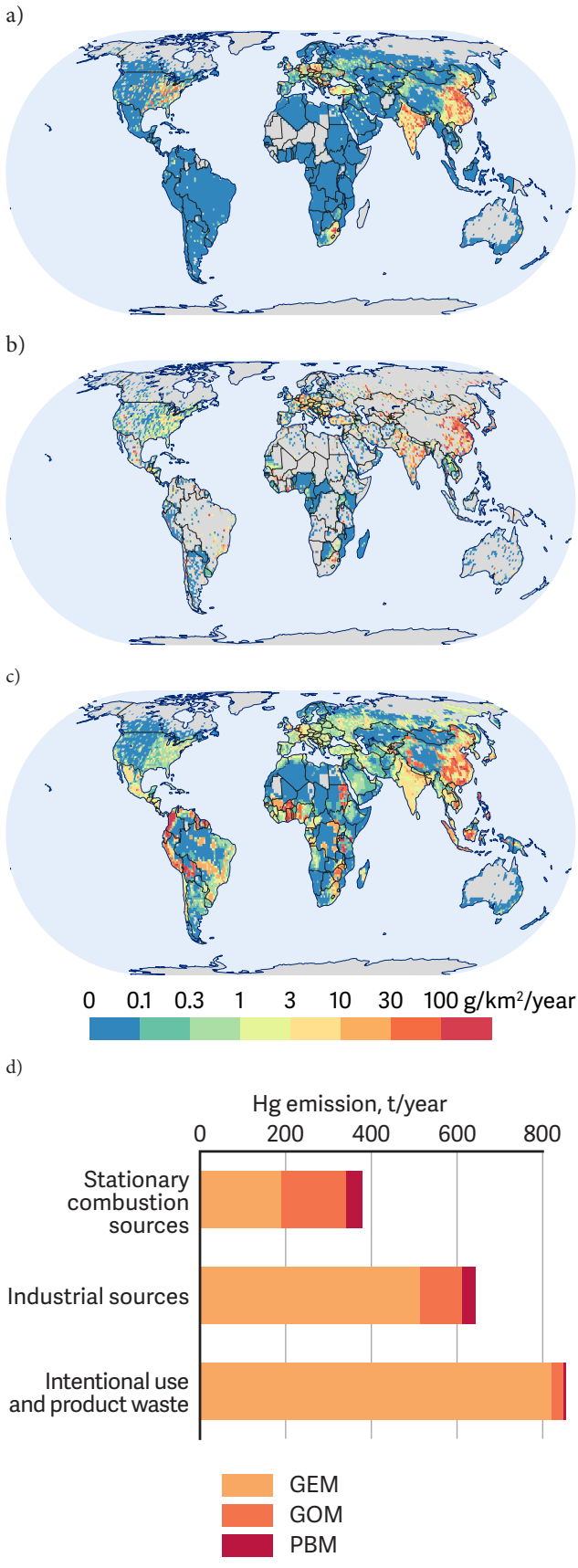

Figure 11. Spatial distribution of mercury emissions from stationary combustion sources (a), industrial sources (b) and intentional use and product waste (c). The chemical speciation of mercury emissions from the three sector groups is shown in 'd'.

The contribution of this sector group varies between 10% and 30% everywhere with the maximum impact occurring in the equatorial zone (Figure 12c).

The sectoral composition of mercury deposition in different geographical regions is illustrated in this figure. It is clear that anthropogenic mercury deposition in the major source regions is largely determined by stationary combustion and industrial sources. These emission sectors dominate in Asia, Europe, North America and the CIS countries. In contrast, regions with lower emissions (Central and South America, Australia and New Zealand, the Arctic etc.) are more affected by mercury from intentional use and product waste associated sectors.

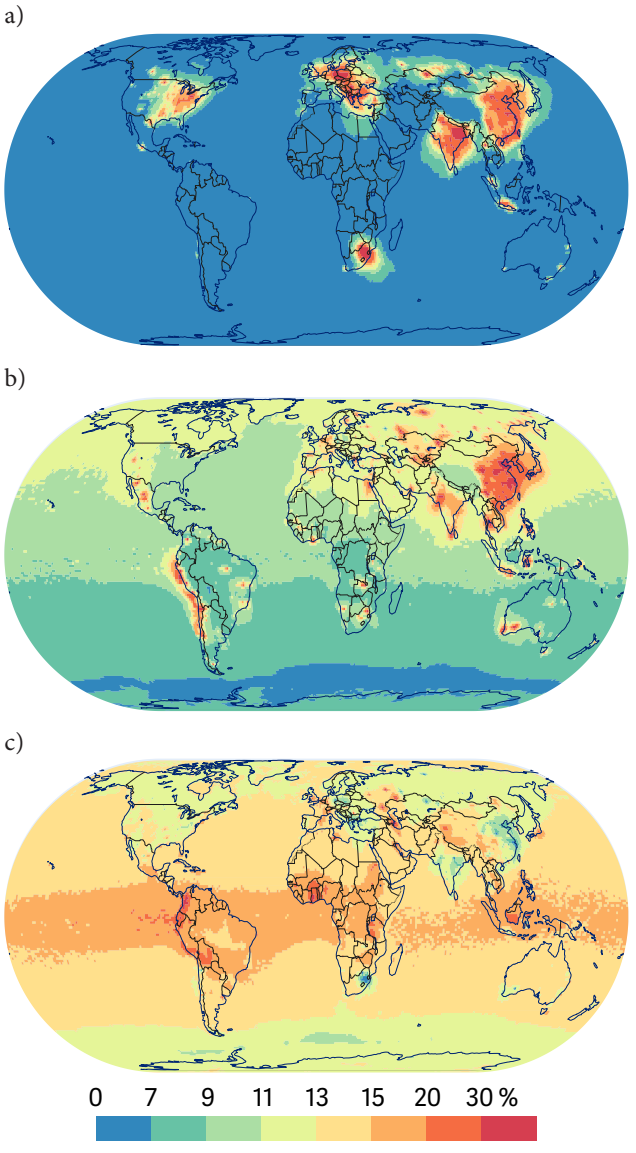

Figure 12. Ensemble mean relative contribution of different groups of emission sectors to total mercury deposition in 2013: stationary combustions sources (a), industrial sources (b) and intentional use and product waste (c).

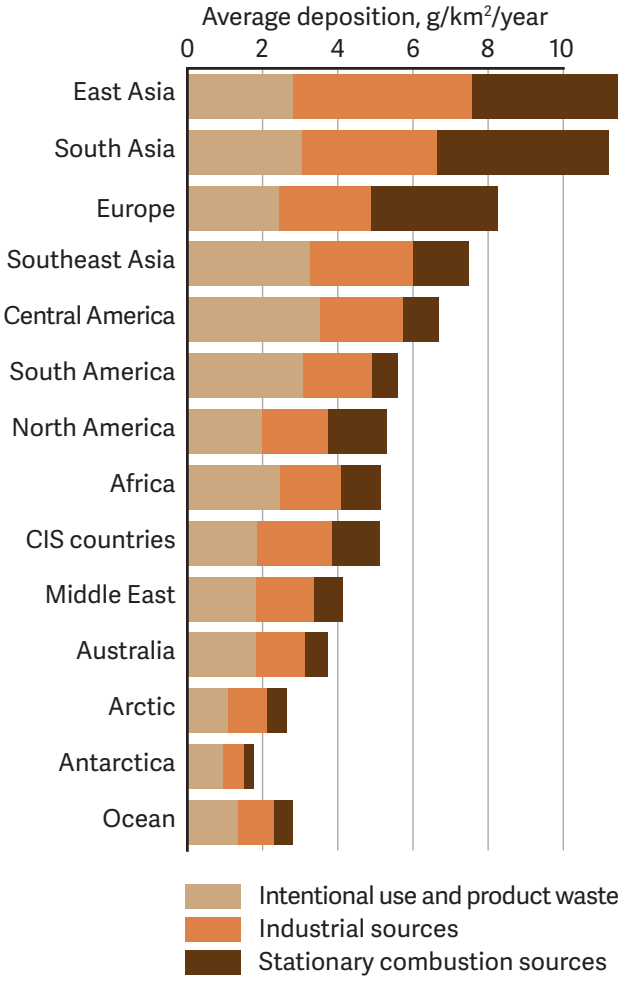

Figure 13. Contribution of mercury emissions from the three sector-specific emission groups to average mercury deposition from contemporary anthropogenic sources in various geographic regions in 2013 as simulated by the model ensemble.

5. Conclusions

The major conclusions of this assessment of mercury atmospheric dispersion and deposition on a global scale and the intercontinental transport and source apportionment of mercury deposition, based on simulation results from an ensemble of global-scale models, may be summarized as follows.

High mercury deposition fluxes are characteristic of the large industrial regions (East and South Asia, Europe, North America etc.) and regions with significant mercury emissions from ASGM (Southeast Asia, Central and South America, Sub-Saharan Africa). Relatively large deposition is also detected over some remote areas of the oceans and in the polar regions.

Mercury deposition in all geographical regions comprises a contribution emitted from the regions' domestic sources, mercury transported into the region from sources located in other regions ('foreign sources'), and a significant contribution from natural and legacy sources. The share of current anthropogenic emissions varies between 20% and 50%. The contribution of natural/legacy sources is generally greater in remote regions with lower atmospheric deposition.

The contribution of domestic sources varies from zero (Antarctica) to 36% (East Asia). In all regions the contribution of foreign sources is within the range 12–30%.

Anthropogenic mercury deposition in Europe is derived almost equally from domestic and foreign emissions. The largest contributors to foreign emissions include East Asia (20%), Africa (8%), CIS countries (5%), and South Asia (3%). The contribution of domestic sources to mercury deposition in North America (23%) is smaller than total contribution from other source regions, the largest of which include East Asia (32%), Africa (12%), CIS countries (6%) and Central America (6%). In contrast, deposition of mercury to East and South Asia is dominated by contributions from domestic sources (76% and 58%, respectively).

Oceanic regions characterized both by significant mercury deposition and by the highest total capture fisheries production include the Northwest Pacific, Western Central Pacific and Northeast Atlantic. Mercury deposition in these regions is mostly determined by emissions from East Asia, Africa, Europe, CIS countries, and South and Southeast Asia.

The simulated seasonal variation in mercury deposition from domestic sources is considerably less than that from foreign and natural/legacy sources and is mostly determined by changes in environmental conditions affecting removal processes. The contribution of foreign sources is greater in summer when mercury oxidation is more intensive. In the case of natural/legacy sources, the seasonal pattern is also affected by the intensity of mercury emission from the surface.

Mercury deposition in industrial regions is largely determined by emissions from stationary combustion and industrial sources. In contrast, regions with lower emissions are more affected by mercury emissions from intentional use and product waste associated sectors.

6. References

AMAP/UNEP, 2013. Technical Background Report for the Global Mercury Assessment 2013. Arctic Monitoring and Assessment Programme, Oslo, Norway / UNEP Chemicals Branch, Geneva, Switzerland. (www.amap.no/documents/download/1265).

AMAP, 2014. Global Anthropogenic Emissions of Mercury to the Atmosphere (www.amap.no/mercury-emissions/datasets).

Amos, H.M., D.J. Jacob, C.D. Holmes, J.A. Fisher, Q. Wang, R.M. Yantosca, E.S. Corbitt, E. Galarneau, A.P. Rutter, M.S. Gustin, A. Steffen, J.J. Schauer, J.A. Graydon, V.L. St Louis, R.W. Talbot, E.S. Edgerton, Y./ Zhang and E.M. Sunderland, 2012. Gas-particle partitioning of atmospheric Hg(II) and its effect on global mercury deposition. Atmospheric Chemistry and Physics, 12:591-603.

Chen, L., H.H. Wang, J.F. Liu, Y.D. Tong, L.B. Ou, W. Zhang, D. Hu, C. Chen and X.J. Wang, 2014. Intercontinental transport and deposition patterns of atmospheric mercury from anthropogenic emissions. Atmospheric Chemistry and Physics, 14:10163-10176.

Corbitt, E.S., D.J. Jacob, C.D. Holmes, D.G. Streets and E.M. Sunderland, 2011. Global source-receptor relationships for mercury deposition under present-day and 2050 emissions scenarios. Environmental Science and Technology, 45:10477-10484.

Cossa, D., B. Averty and N. Pirrone, 2009. The origin of methylmercury in open Mediterranean waters. Limnology and Oceanography, 54:837-844.

Dastoor, A., A. Ryzhkov, D. Durnford, I. Lehnherr, A. Steffen and H. Morrison, 2015. Atmospheric mercury in the Canadian Arctic Part II: Insight from modeling. Science of the Total Environment, in press.

Durnford, D., A. Dastoor, A. Ryzhkov, L. Poissant, M. Pilote and D. Figueras-Nieto, 2012. How relevant is the deposition of mercury onto snowpacks? Part 2: A modeling study. Atmospheric Chemistry and Physics, 12:9251-9274.

FAO, 2014a. Search Geographical Information. FAO Major Fishing Areas. UN Food and Agriculture Organization (www.fao.org/fishery/area/search/en).

FAO, 2014b. Fishery Statistical Collections. Global Capture Production. UN Food and Agriculture Organization (www.fao.org/fishery/statistics/global-capture-production/en).

Holmes, C., D. Jacob, E. Corbitt, J. Mao, X. Yang, R. Talbot and F. Slemr. 2010. Global atmospheric model for mercury including oxidation by bromine atoms. Atmospheric Chemistry and Physics, 10:12037-12057.

Kos, G., A. Ryzhkov, A. Dastoor, J. Narayan, A. Steffen, P.A. Ariya and L. Zhang, 2013. Evaluation of discrepancy between measured and modelled oxidized mercury species. Atmospheric Chemistry and Physics, 13:4839-4863.

Lei, H., X.-Z. Liang, D.J. Wuebbles and Z. Tao, 2013. Model analyses of atmospheric mercury: present air quality and effects of transpacific transport on the United States. Atmospheric Chemistry and Physics, 13:10807-10825.

Mahaffey, K.R., R.P. Clickner and C.C. Bodurow, 2004. Blood organic mercury and dietary mercury intake: National Health and Nutrition Examination Survey, 1999 and 2000. Environmental Health Perspectives, 112:562-670.

Mahaffey K., R.P. Clickner and R.A. Jeffries, 2009. Adult women's blood mercury concentrations vary regionally in USA: Association with patterns of fish consumption (NHANES 1999-2004). Environmental Health Perspectives, 117:47-53.

Mason, R.P., A.L. Choi, W.F. Fitzgerald, C.R. Hammerschmidt, C.H. Lamborg, A.L. Soerensen and E.M. Sunderland, 2012. Mercury biogeochemical cycling in the ocean and policy implications. Environmental Research, 119:101-117.

Seigneur, C., K. Vijayaraghavan, K. Lohman, P. Karamchandani and C. Scott, 2004. Global source attribution for mercury deposition in the United States. Environmental Science and Technology, 38:555-569.

Selin, N.E., 2009. Global biogeochemical cycling of mercury: A review. Annual Review of Environment and Resources, 34:43-63.

Selin, N.E., D.J. Jacob, R.M. Yantosca, S. Strode, L. Jaegle and E.M. Sunderland, 2008. Global 3-D land-ocean-atmosphere model for mercury: Present-day versus preindustrial cycles and anthropogenic enrichment factors for deposition. Global Biogeochemical Cycles, 22:GB2011, doi: 10.1029/2007GB003040.

Sunderland, E.M., F.A.P.C. Gobas, A. Heyes, B.A. Branfireun, A.K. Bayer, R.E. Cranston and M.B. Parsons, 2004. Speciation and bioavailability of mercury in well-mixed estuarine sediments. Marine Chemistry, 90:91-105.

Sunderland, E.M., D.P. Krabbenhoft, J.W. Moreau, S.A. Strode and W.M. Landing, 2009. Mercury sources, distribution, and bioavailability in the North Pacific Ocean: Insights from data and models. Global Biogeochemical Cycles, 23:GB2010, doi: *10.1029/2008GB003425*.

Sunderland, E., E. Corbitt, D. Cossa, D. Evers, H. Friedli, D. Krabbenhoft, L. Levin, N. Pirrone and G. Rice, 2010. Impacts of intercontinental mercury transport on human and ecological health. In: Pirrone, N. and T. Keating (eds.), Hemispheric Transport of Air Pollution 2010. Part B: Mercury, pp. 97-144. Air Pollution Studies No. 16. United Nations.

Travnikov, O., 2011. Atmospheric transport of mercury. In: Liu, G., Y. Cai and N. O'Driscoll (eds.), Environmental Chemistry and Toxicology of Mercury. John Wiley & Sons.

Travnikov O. and I. Ilyin, 2009. The EMEP/MSC-E mercury modeling system. In: Pirrone, N. and R.P. Mason (eds.), Mercury Fate and Transport in the Global Atmosphere: Emissions, Measurements, and Models. pp. 571-587. Springer.

Travnikov, O., J.E. Jonson, A.S. Andersen, M. Gauss, A. Gusev, O. Rozovskaya, D. Simpson, V. Sokovyh, S. Valiyaveetil and P. Wind, 2009. Development of the EMEP global modelling framework: Progress report. Available: http://www.msceast.org/index.php/reports.

Wiener, J.G., D.P. Krabbenhoft, G.H. Heinz and A.M. Scheuhammer, 2003. Ecotoxicology of mercury. In: Hoffman, D.J., B.A. Rattner, G.A. Burton, Jr. and J. Cairns, Jr. (eds.), Handbook of Ecotoxicology. pp. 407-461, CRC Press.

Zhang, L., P. Blanchard, D. Johnson, A. Dastoor, A. Ryzhkov, C.-J. Lin, K. Vijayaraghavan, D. Gay, T.M. Holsen, J. Huang, J.A. Graydon, V.L. St. Louis, M.S. Castro, E.K. Miller, F. Marsik, J. Lu, L. Poissant, M. Pilote and K.M. Zhang, 2012. Assessment of modeled mercury deposition over the Great Lakes region. Environmental Pollution, 161:272-283.

Annex A. Model ensemble

Table A-1. Characteristics of chemical transport models participated in the multi-model experiments.

Characteristics	GMHG[a]	GEOS-Chem	GLEMOS
Institution	Environment Canada	Massachusetts Institute of Technology	Meteorological Synthesizing Centre - East
Domain	Global	Global	Global
Spatial resolution			
Horizontal	1° × 1°	2.5° × 2°	1° × 1°
Vertical	58 levels, top 7 hPa	47 levels, top 0.01 hPa	20 levels, top 10 hPa
Type	Atmospheric	Multi-media	Atmospheric
Emissions			
Anthropogenic, t/y	1875	1875	1875
Speciation (average), GEM : GOM : PBM	96 : 3 : 1	81 : 19 : 0	81 : 15 : 4
Natural and legacy, t/y	3660	5070	3995
Atmospheric chemistry			
Oxidation (air)	OH	Br	OH, O3, Cl2
Reduction (air)	none	none	none
Oxidation (cloud water)	none	none	OH, O3, HOCl/OCl-
Reduction (cloud water)	none	none	SO32-
Remarks	Parameterization of AMDEs based on Br chemistry, re-emission from snow	Gas-particle partitioning of Hg(II). Parameterization of AMDEs based on Br chemistry, re-emission from snow	Parameterization of AMDEs based on Br chemistry, re-emission from snow, chemical reactants imported from MOZART and p-TOMCAT
References	Durnford at al. (2012); Kos et al. (2013); Dastoor et al. (2015)	Holmes et al. (2010); Amos et al. (2012)	Travnikov et al. (2009)

[a] GMHG is a new chemical transport model for mercury that is based on the GRAHM model developed by Environment Canada.

Annex B. Simulation results for the individual chemical transport models

B.1. Spatial distribution of mercury air concentrations and deposition

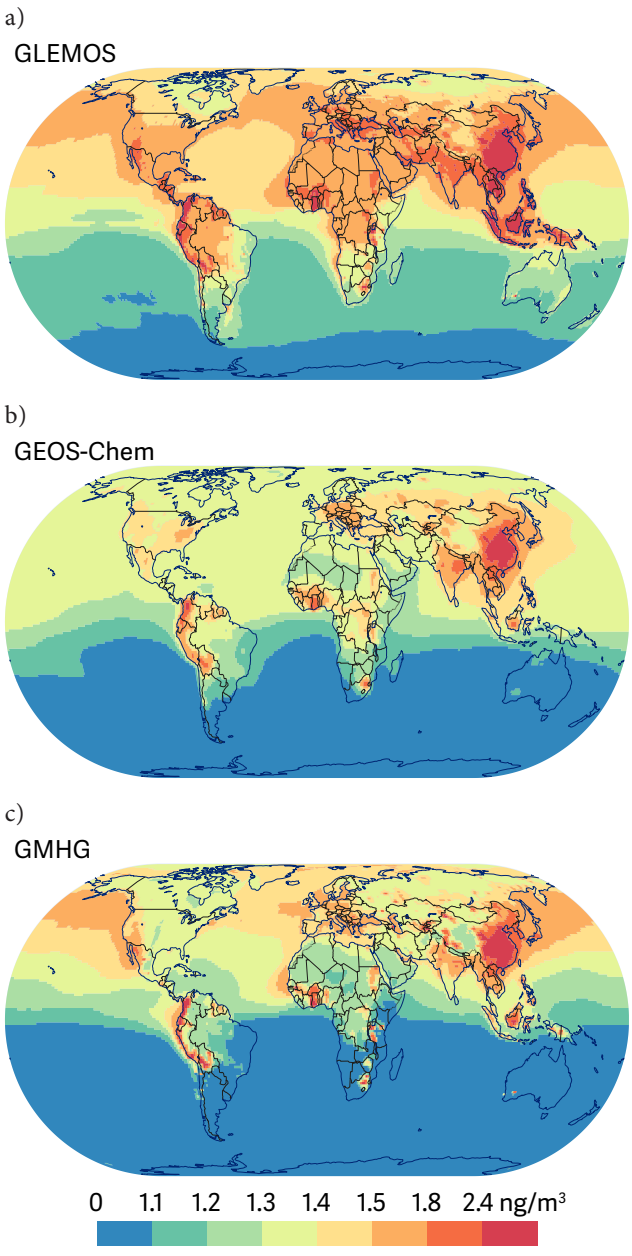

Figure B-1. Spatial distribution of annual mean gaseous elemental mercury (GEM) concentration in ambient air in 2013 as simulated by the three chemical transport models.

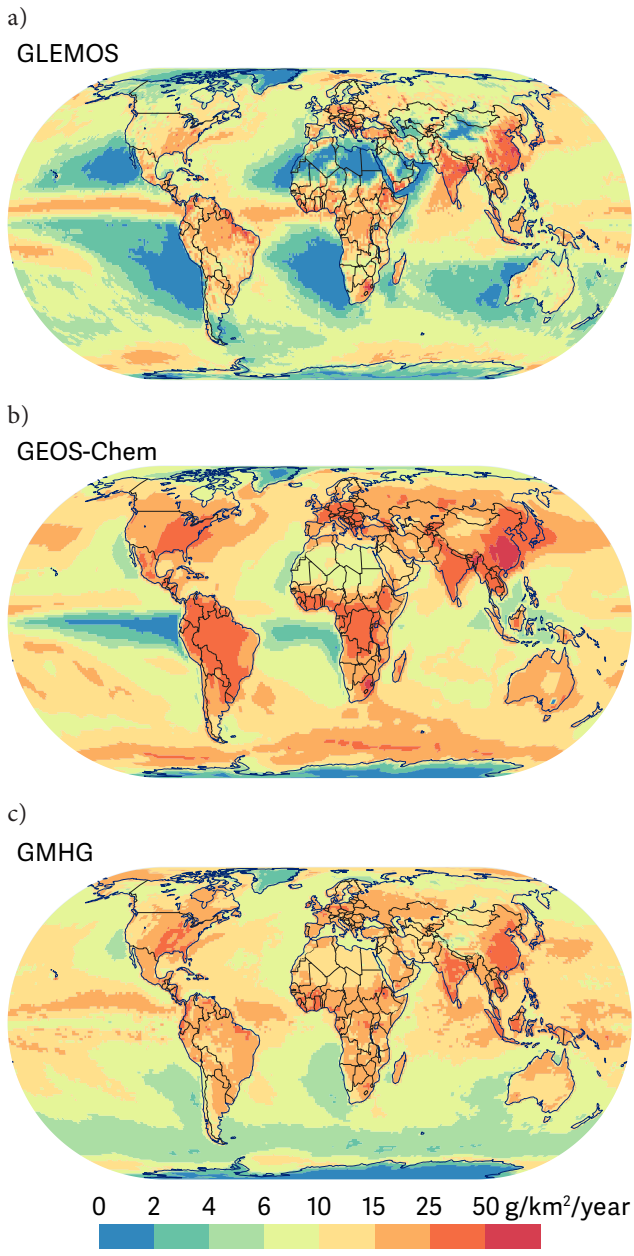

Figure B-2. Spatial distribution of total mercury (dry and wet) deposition in 2013 as simulated by the three chemical transport models.

B.2. Source attribution for atmospheric mercury deposition

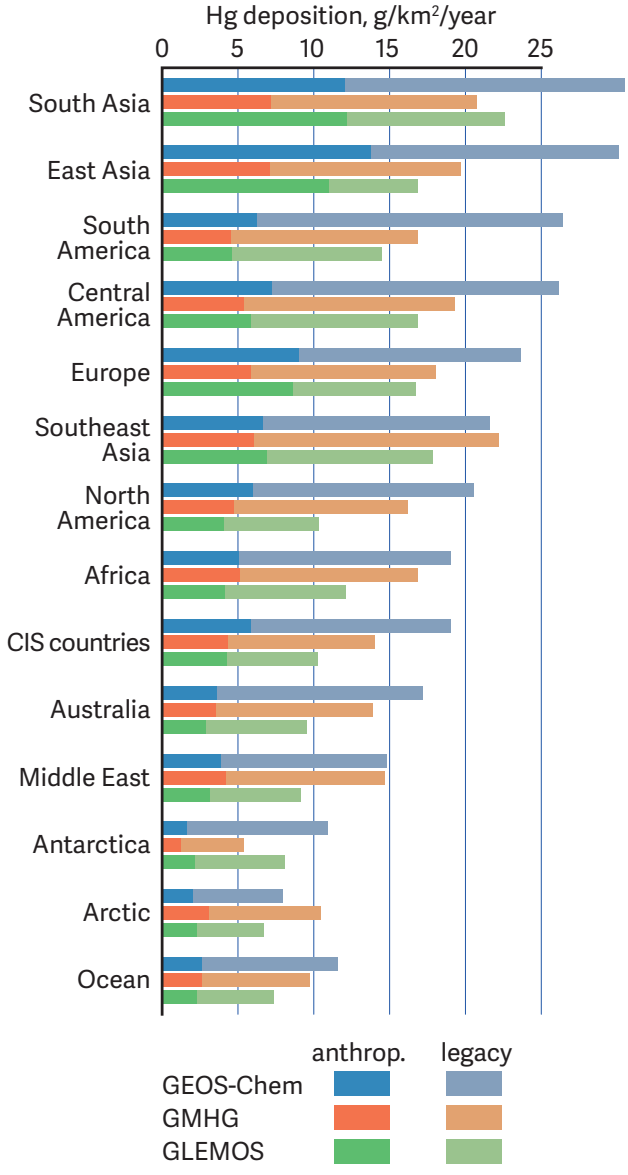

Figure B-3. Average mercury deposition flux in various geographical regions in 2013 as simulated by the three chemical transport models.

Table B-1. Nomenclature of sources and receptors

	Code	Description
Terrestrial regions	NAM	North America
	EUR	Europe
	SAS	South Asia
	EAS	East Asia
	SEA	Southeast Asia
	PAN	Australia and New Zealand
	AFR	Africa
	MDE	Middle East
	MCA	Central America
	SAM	South America
	CIS	CIS countries
	ARC	Arctic
	ANT	Antarctic
Aquatic regions	ARS	Arctic Sea
	MED	Mediterranean and Black Seas
	ATL	Atlantic Ocean
	PAC	Pacific Ocean
	IND	Indian Ocean
	STH	Southern Ocean
	NAT	Natural / legacy sources

Table B-2. Source-receptor deposition matrix simulated by GLEMOS, tonnes/year

	Area, km²	NAM	EUR	SAS	EAS	SEA	PAN	AFR	MDE	MCA	SAM	CIS	ARC	NAT	Total
Deposition to terrestrial regions															
NAM	1.69×10^7	**21.8**	3.0	3.1	18.4	3.7	0.3	7.3	0.5	4.1	3.2	3.5	0.3	105.4	174.6
EUR	5.53×10^6	0.7	**29.1**	1.2	7.0	1.5	0.1	3.4	0.3	1.2	1.3	1.9	0.1	44.5	92.3
SAS	5.07×10^6	0.6	1.2	**41.6**	7.1	1.9	0.2	3.9	0.6	1.5	1.8	1.4	0.1	52.6	114.4
EAS	1.16×10^7	0.8	1.7	3.1	**106.4**	3.2	0.2	4.6	0.4	1.8	2.0	2.8	0.2	67.5	194.7
SEA	4.94×10^6	0.5	1.0	2.5	8.9	**12.9**	0.2	3.6	0.2	1.4	1.9	1.1	0.1	54.0	88.2
PAN	8.06×10^6	0.4	0.8	1.3	5.4	2.1	**3.5**	4.4	0.2	1.6	2.7	0.9	0.1	53.5	76.9
AFR	3.00×10^7	2.3	6.2	6.9	28.5	8.4	1.0	**48.8**	1.7	6.8	9.5	5.0	0.4	238.1	363.6
MDE	5.17×10^6	0.4	1.4	1.0	4.3	1.0	0.1	2.6	**2.7**	0.9	1.0	1.0	0.1	30.7	47.1
MCA	5.21×10^6	1.0	1.2	1.5	7.5	2.0	0.2	4.8	0.3	**8.1**	2.4	1.3	0.1	57.2	87.7
SAM	1.53×10^7	1.2	2.6	3.7	16.1	5.4	0.7	13.4	0.6	5.4	**18.2**	2.7	0.2	151.1	221.3
CIS	1.79×10^7	1.7	6.7	3.1	21.1	3.6	0.4	7.4	0.9	3.0	3.2	**25.2**	0.6	107.3	184.1
ARC	2.24×10^7	1.7	4.3	2.9	18.6	3.4	0.3	6.9	0.6	2.8	3.0	5.2	**1.8**	97.5	148.9
ANT	3.42×10^7	1.4	3.1	4.4	19.2	7.1	1.5	16.2	0.7	5.7	10.8	3.2	0.2	202.5	276.0
Deposition to aquatic regions															
ARS	9.25×10^6	0.8	1.5	1.1	7.1	1.3	0.1	2.6	0.2	1.1	1.1	1.9	0.4	36.8	55.9
MED	2.99×10^6	0.2	3.3	0.3	1.7	0.4	0	1.3	0.2	0.3	0.3	0.5	0	11.4	20.2
ATL	8.53×10^7	8.8	13.6	11.5	59.1	15.1	1.7	37.5	2.0	13.6	18.3	11.3	1.1	428.2	621.9
PAC	1.69×10^8	9.2	18.8	24.2	149.2	39.5	5.1	68.6	3.9	28.7	40.3	21.9	1.8	883.7	1294.9
IND	6.06×10^7	2.3	5.0	17.8	32.4	12.6	3.0	26.8	1.8	8.2	13.5	5.2	0.4	283.1	412.3
STH	3.55×10^7	1.8	3.8	5.4	23.6	8.7	1.8	20.5	0.9	7.0	13.3	3.9	0.3	246.4	337.6

Table B-3. Source-receptor deposition matrix simulated by GEOS-Chem, tonnes/year

	Area, km²	NAM	EUR	SAS	EAS	SEA	PAN	AFR	MDE	MCA	SAM	CIS	ARC	NAT	Total
Deposition to terrestrial regions															
NAM	1.69×10^7	**25.0**	4.7	5.1	32.3	4.3	0.3	11.5	0.9	6.4	4.6	6.1	0.4	246.2	347.8
EUR	5.53×10^6	1.0	**26.3**	1.6	9.8	1.3	0.1	3.8	0.4	1.5	1.4	2.5	0.1	80.8	130.7
SAS	5.07×10^6	0.7	1.3	**36.8**	9.0	1.9	0.2	4.9	0.7	1.9	2.1	1.6	0.1	93.4	154.6
EAS	1.16×10^7	1.7	3.2	5.9	**122.1**	4.3	0.3	8.7	0.7	3.5	3.6	5.8	0.3	188.7	348.6
SEA	4.94×10^6	0.5	0.9	3.1	10.6	**9.5**	0.2	3.8	0.2	1.4	1.8	1.0	0.1	73.6	106.7
PAN	8.06×10^6	0.5	1.0	1.7	6.6	2.2	**3.0**	6.6	0.2	2.2	4.1	1.0	0.1	109.2	138.3
AFR	3.00×10^7	2.9	6.8	8.4	34.3	8.5	0.9	**62.2**	1.6	8.9	12.2	5.7	0.3	419.2	572.1
MDE	5.17×10^6	0.5	1.5	1.4	6.1	1.1	0.1	3.3	**2.2**	1.2	1.3	1.3	0.1	56.3	76.5
MCA	5.21×10^6	1.0	1.4	2.0	9.0	1.9	0.2	6.6	0.3	**10.7**	3.0	1.5	0.1	98.4	136.0
SAM	1.53×10^7	1.7	3.1	5.0	20.3	6.0	0.8	20.3	0.7	7.9	**26.4**	3.2	0.2	308.2	403.9
CIS	1.79×10^7	2.9	9.6	4.6	34.3	3.9	0.3	10.3	1.3	4.3	4.0	**28.7**	0.8	236.1	341.2
ARC	2.24×10^7	1.8	3.8	2.4	18.2	2.1	0.2	5.6	0.5	2.3	2.2	5.4	**1.6**	132.0	178.0
ANT	3.42×10^7	1.0	1.9	3.2	12.6	4.2	1.3	14.6	0.5	4.7	10.0	2.0	0.1	315.6	371.7
Deposition to aquatic regions															
ARS	9.25×10^6	0.7	1.3	0.9	6.6	0.7	0.1	2.0	0.2	0.8	0.8	1.9	0.4	47.7	64.0
MED	2.99×10^6	0.3	5.9	0.6	3.5	0.6	0	1.9	0.2	0.6	0.6	1.0	0	30.3	45.8
ATL	8.53×10^7	9.6	15.1	14.6	70.3	15.0	1.7	44.6	2.3	16.9	22.4	12.5	1.0	736.9	962.8
PAC	1.69×10^8	10.3	18.1	28.6	164.4	34.0	4.5	82.5	4.2	32.6	44.9	22.3	1.3	1437.8	1885.4
IND	6.06×10^7	2.9	5.3	20.4	36.5	12.3	2.8	37.7	2.0	11.4	18.6	5.7	0.3	530.1	686.1
STH	3.55×10^7	1.7	3.1	5.2	20.5	6.9	2.0	23.6	0.8	7.5	16.0	3.3	0.2	501.0	591.9

Table B-4. Source-receptor deposition matrix simulated by GMHG, tonnes/year

	Area, km²	NAM	EUR	SAS	EAS	SEA	PAN	AFR	MDE	MCA	SAM	CIS	ARC	NAT	Total
Deposition to terrestrial regions															
NAM	1.69×10^7	**10.0**	5.0	5.1	30.1	3.0	0.4	10.1	0.8	4.8	4.7	6.2	0.5	193.1	273.7
EUR	5.53×10^6	1.3	**9.9**	1.7	9.6	1.0	0.1	3.4	0.3	1.4	1.5	2.4	0.2	67.3	99.9
SAS	5.07×10^6	0.8	1.3	**14.2**	8.6	1.3	0.2	4.4	0.5	1.6	2.0	1.5	0.1	68.7	105.1
EAS	1.16×10^7	1.8	3.0	4.3	**52.7**	2.5	0.3	7.1	0.6	2.9	3.3	4.4	0.3	145.0	228.0
SEA	4.94×10^6	0.7	1.1	2.7	10.2	**4.2**	0.3	5.0	0.3	1.8	2.5	1.3	0.1	79.5	109.6
PAN	8.06×10^6	0.7	1.0	2.0	7.4	1.7	**1.5**	6.8	0.2	2.2	4.1	1.1	0.1	83.3	112.0
AFR	3.00×10^7	4.3	8.1	10.6	40.3	6.6	1.1	**52.5**	1.4	8.9	12.6	6.7	0.4	351.7	505.2
MDE	5.17×10^6	0.8	1.7	2.0	7.4	1.0	0.1	3.6	**1.0**	1.3	1.5	1.5	0.1	54.0	76.0
MCA	5.21×10^6	1.0	1.3	1.9	8.1	1.2	0.2	5.8	0.2	**4.7**	2.3	1.3	0.1	72.2	100.4
SAM	1.53×10^7	1.7	2.5	4.7	17.2	3.5	0.8	16.8	0.5	5.4	**13.8**	2.6	0.2	188.0	257.6
CIS	1.79×10^7	3.2	7.5	4.3	27.2	2.5	0.3	8.3	0.8	3.6	3.8	**16.1**	0.8	173.7	252.3
ARC	2.24×10^7	3.3	6.1	4.0	27.4	2.4	0.3	7.8	0.7	3.6	3.7	8.2	**1.6**	164.9	233.9
ANT	3.42×10^7	1.0	1.5	3.0	10.9	2.5	1.0	10.6	0.3	3.3	6.6	1.6	0.1	141.4	183.8
Deposition to aquatic regions															
ARS	9.25×10^6	2.0	3.5	2.3	15.8	1.3	0.1	4.4	0.4	2.1	2.1	4.8	0.8	91.8	131.3
MED	2.99×10^6	0.4	1.7	0.6	3.0	0.3	0	1.2	0.1	0.5	0.5	0.7	0	21.5	30.6
ATL	8.53×10^7	8.9	13.1	16.2	72.7	10.8	1.9	47.4	2.1	15.5	21.4	13.0	1.1	588.3	812.1
PAC	1.69×10^8	14.1	21.1	35.2	158.0	26.8	4.8	89.0	4.2	38.7	54.1	24.5	1.6	1258.4	1730.4
IND	6.06×10^7	4.0	6.2	16.4	43.8	9.5	2.3	35.8	1.6	11.2	18.5	6.4	0.4	416.6	572.6
STH	3.55×10^7	1.2	1.9	3.7	13.6	3.1	1.2	13.1	0.4	4.1	8.1	2.0	0.1	172.4	225.0

a) GLEMOS

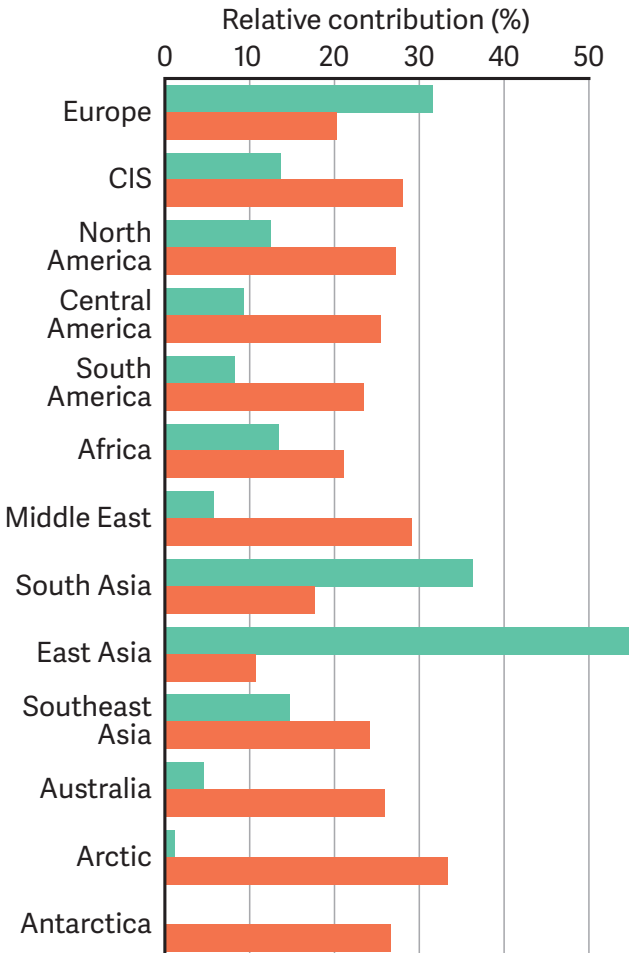

b) GEOS-Chem

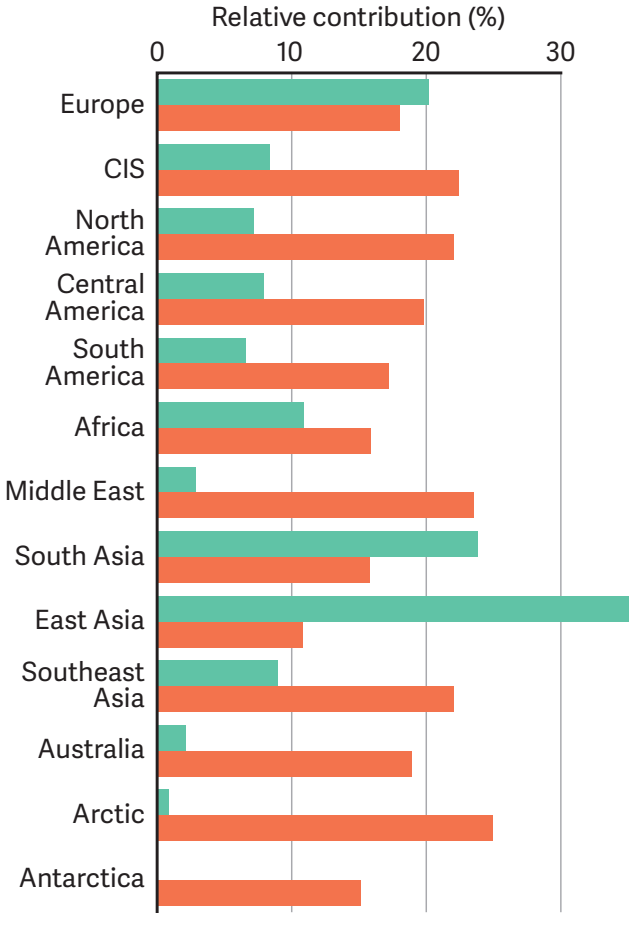

c)GMHG

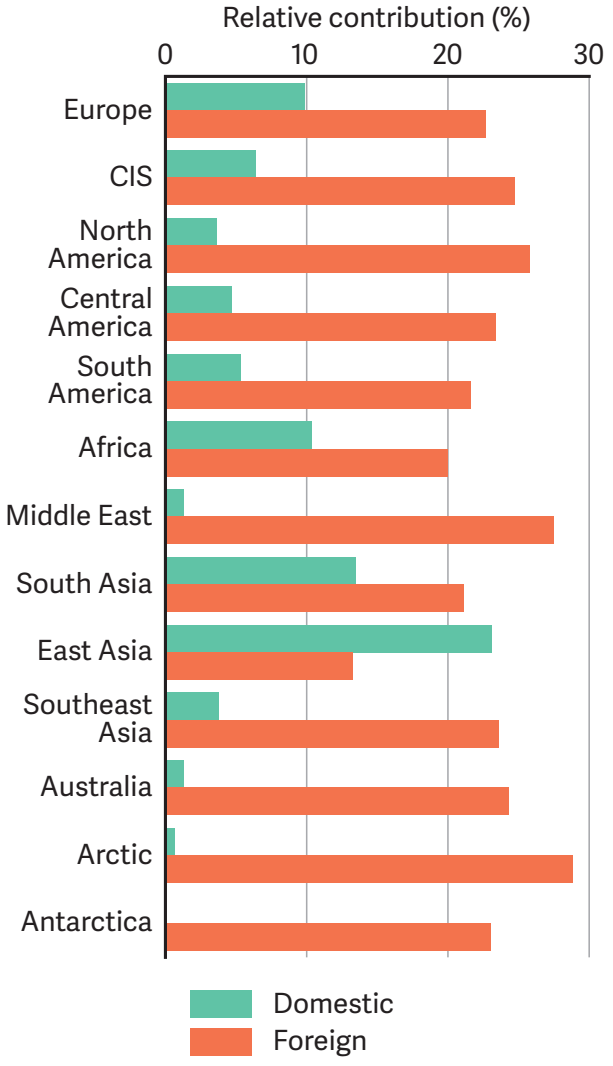

Figure B-4. Relative contribution of domestic and foreign anthropogenic sources to average mercury deposition over various regions in 2013.

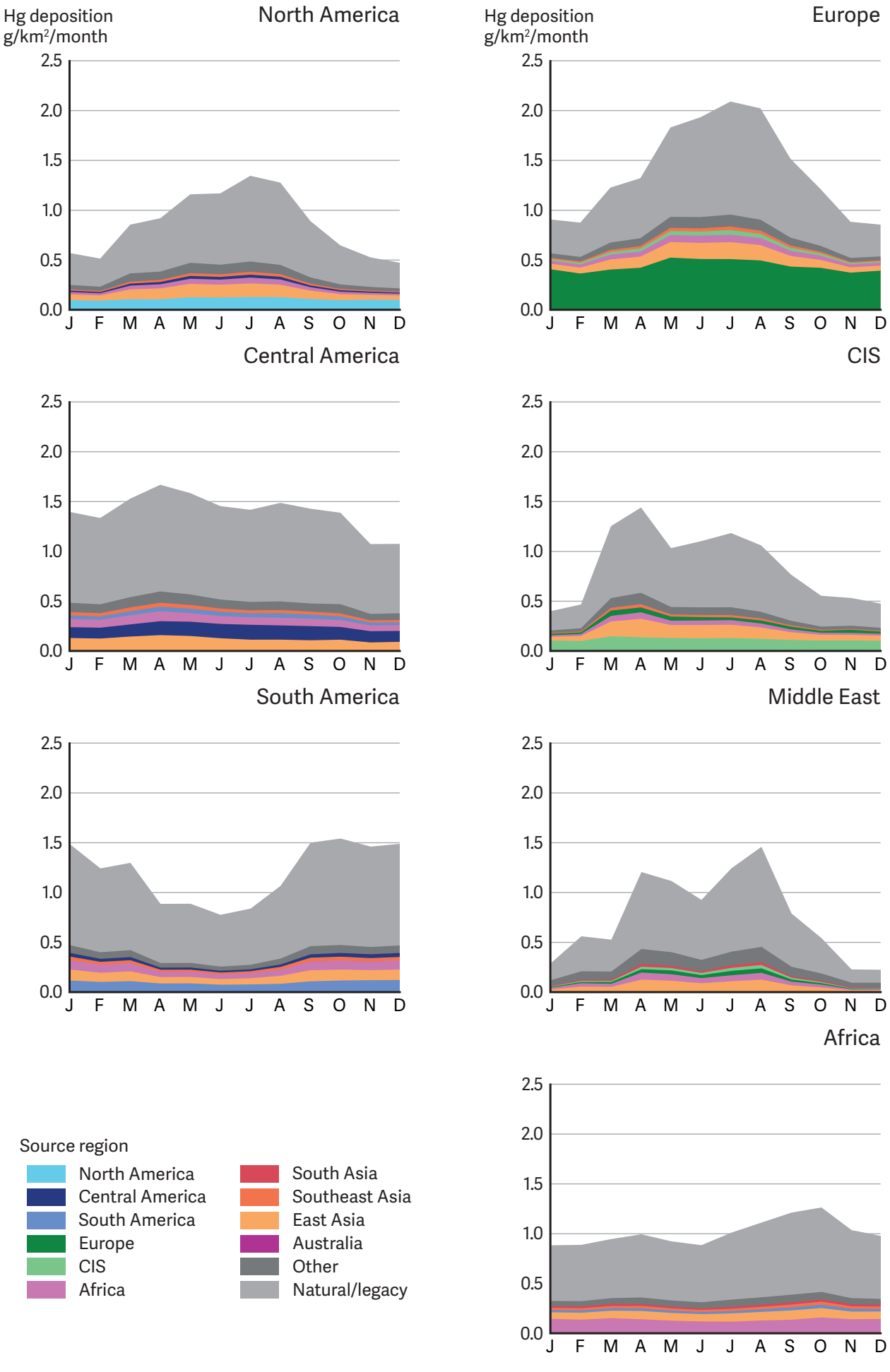
Hg deposition
g/km²/month
North America
Europe
Central America
CIS
South America
Middle East
Africa
2.5
2.0
1.5
1.0
0.5
0.0
J F M A M J J A S O N D
Source region
North America
Central America
South America
Europe
CIS
Africa
South Asia
Southeast Asia
East Asia
Australia
Other
Natural/legacy

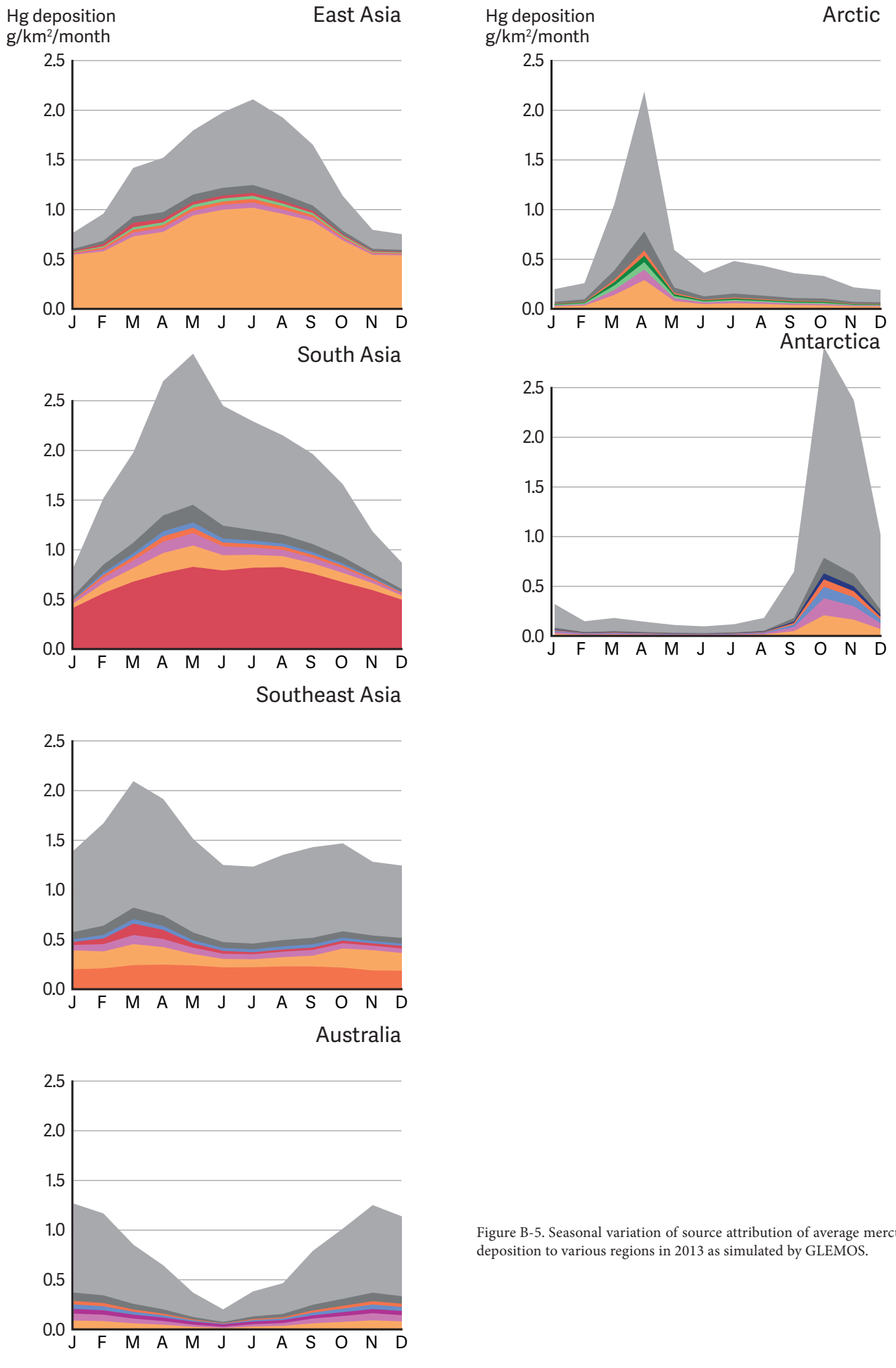

Figure B-5. Seasonal variation of source attribution of average mercury deposition to various regions in 2013 as simulated by GLEMOS.

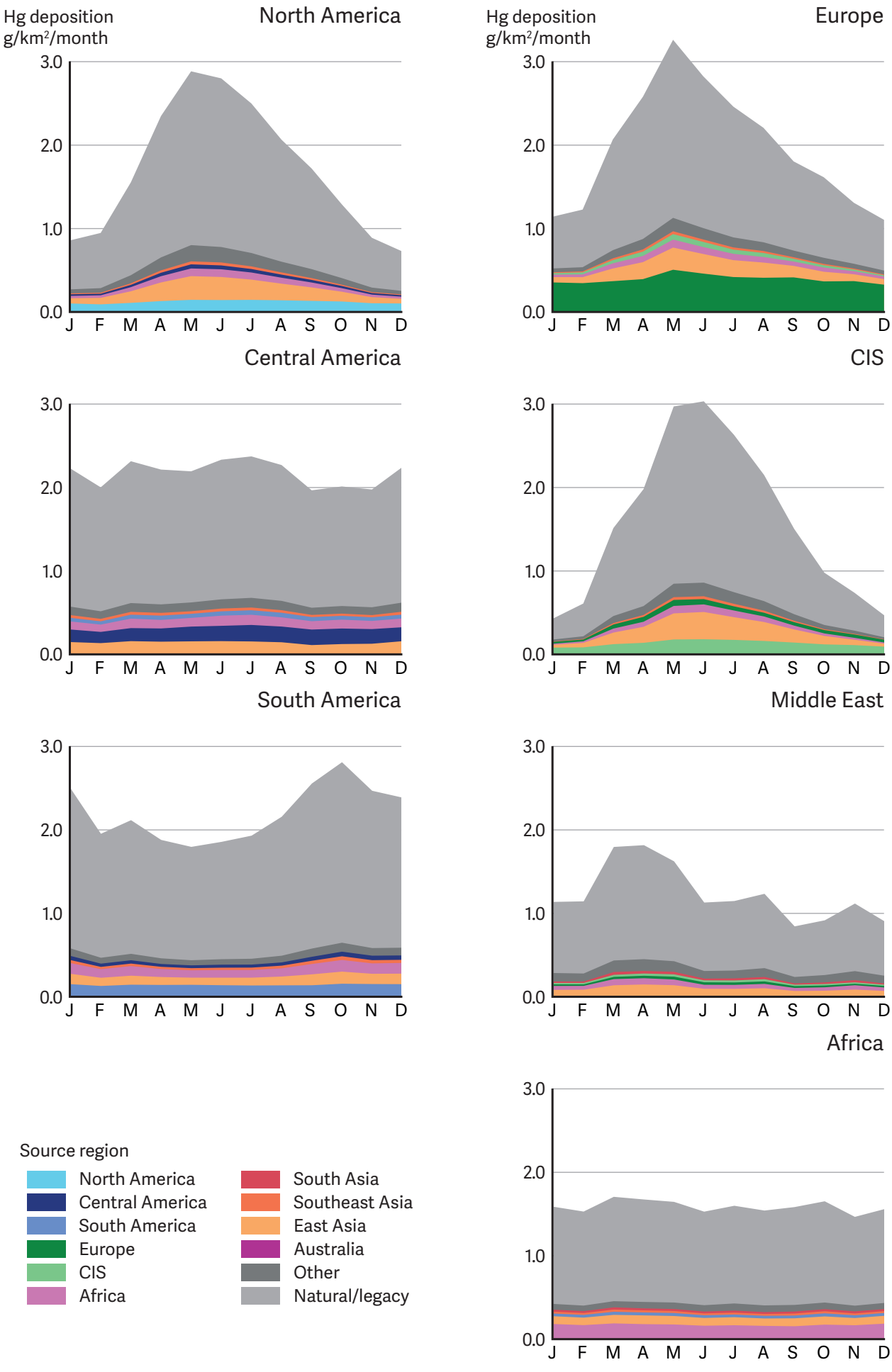
Hg deposition
g/km²/month
North America
Europe
Central America
CIS
South America
Middle East
Africa
3.0
2.0
1.0
0.0
J F M A M J J A S O N D
Source region
North America
Central America
South America
Europe
CIS
Africa
South Asia
Southeast Asia
East Asia
Australia
Other
Natural/legacy

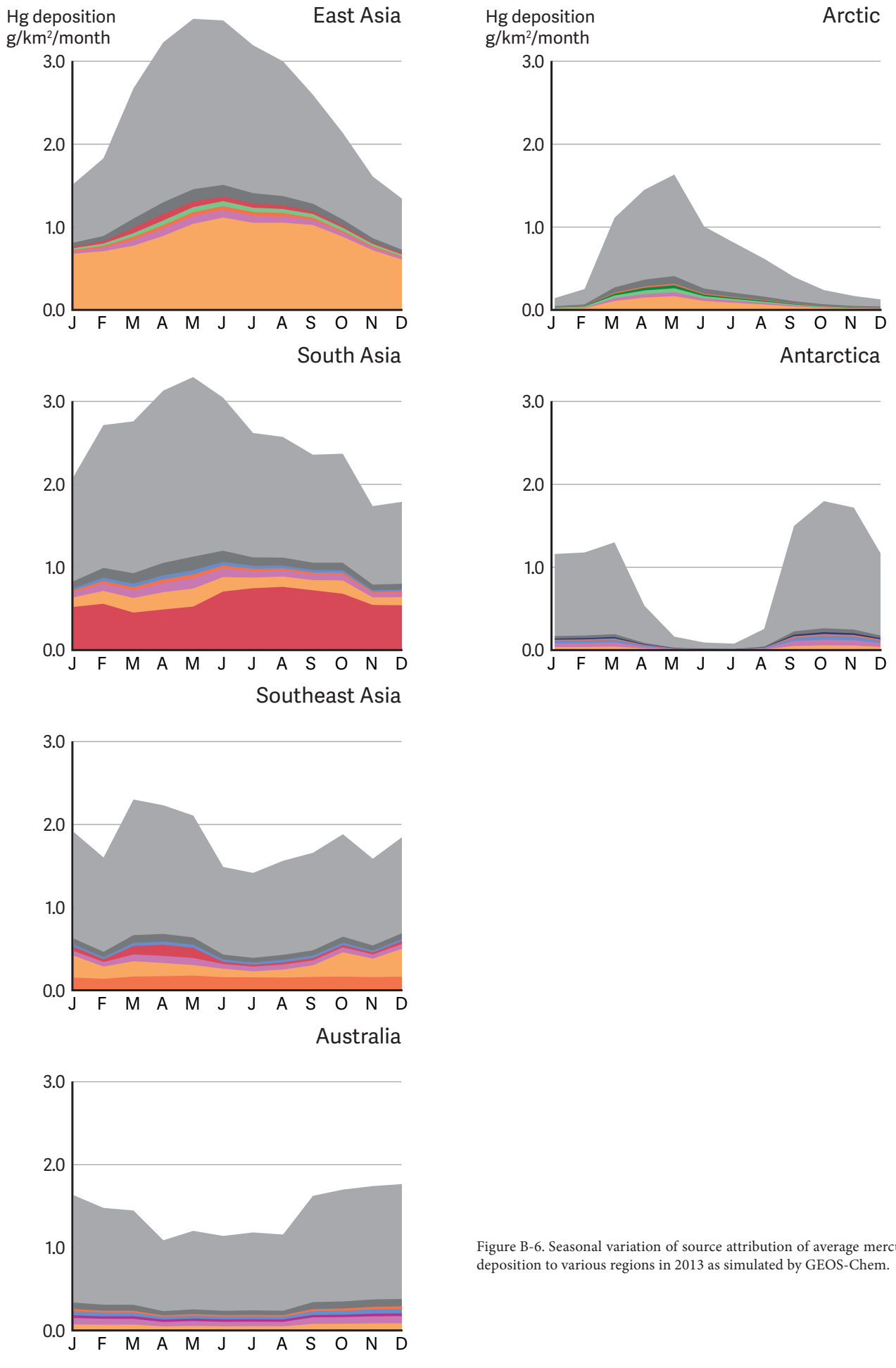

Figure B-6. Seasonal variation of source attribution of average mercury deposition to various regions in 2013 as simulated by GEOS-Chem.

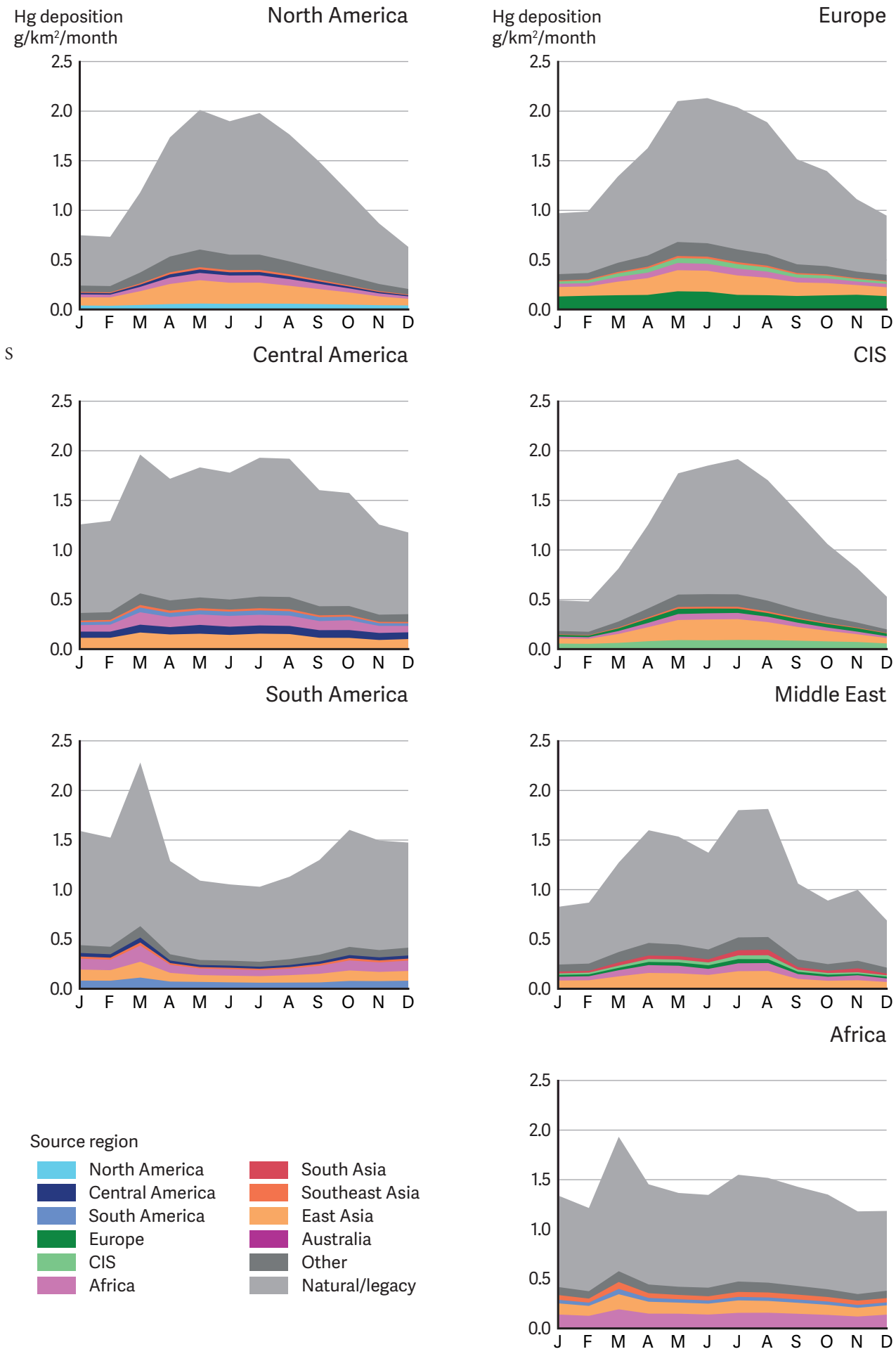
Hg deposition
g/km²/month
North America
Europe
Central America
CIS
South America
Middle East
Africa
2.5
2.0
1.5
1.0
0.5
0.0
J F M A M J J A S O N D
Source region
North America
Central America
South America
Europe
CIS
Africa
South Asia
Southeast Asia
East Asia
Australia
Other
Natural/legacy

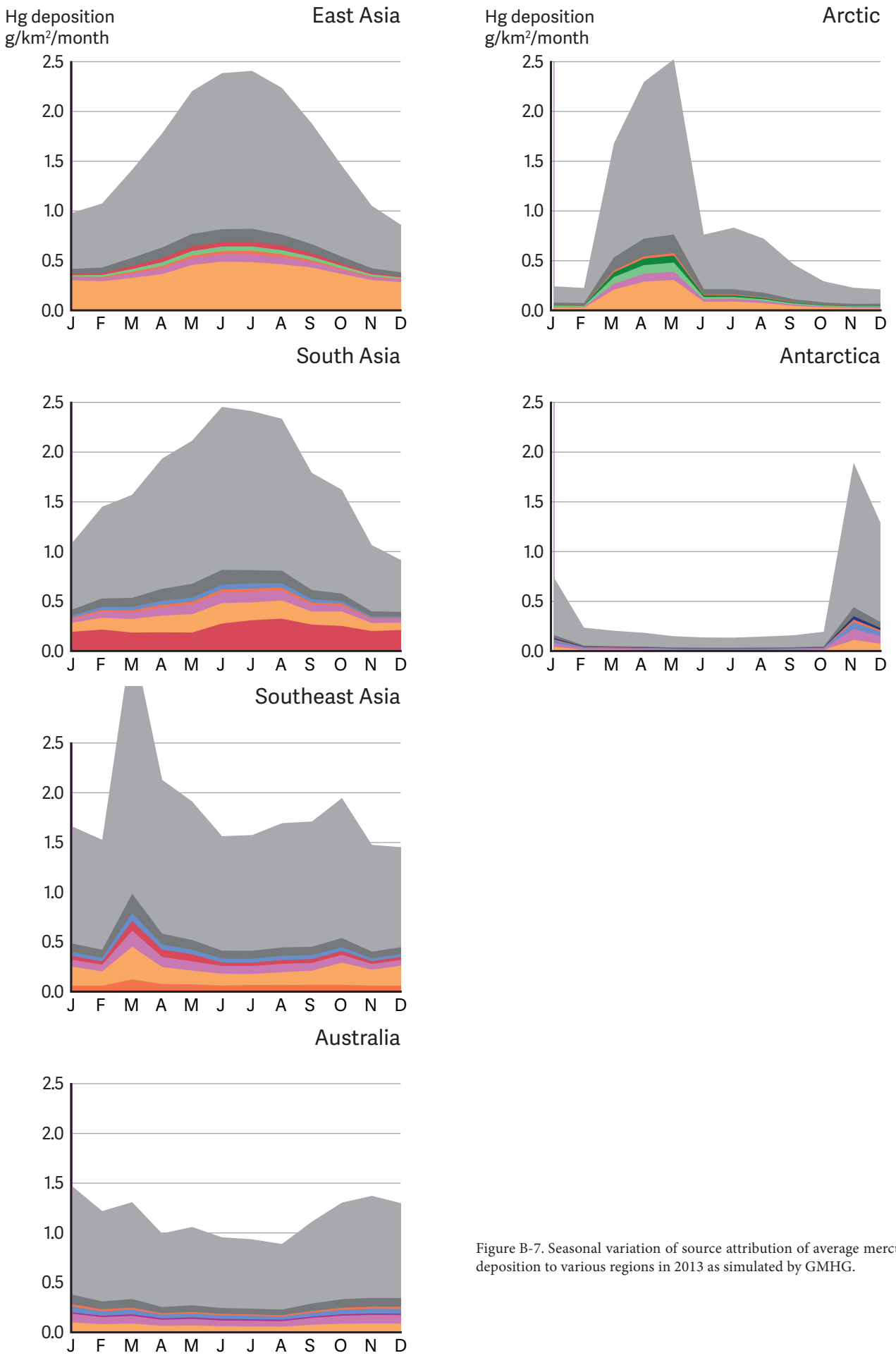

Figure B-7. Seasonal variation of source attribution of average mercury deposition to various regions in 2013 as simulated by GMHG.

B.3. Mercury deposition from different emission sectors

Table B-5. Definition of groups of emission sectors

Sector code	Description
Stationary combustion sources (power plants and distributed heating and energy uses excluding industrial uses)	
SC-PP-coal	Coal combustion in power plants
SC-PP-oil	Oil combustion in power plants
SC-PP-gas	Natural gas combustion in power plants
SC-DR-coal	Coal combustion in domestic residential and other uses
SC-DR-oil	Oil combustion in domestic residential and other uses
SC-DR-gas	Natural gas combustion in domestic residential and other uses
Industrial sources (including stationary combustion for industry)	
SC-IND-coal	Coal combustion in industry
SC-IND-oil	Oil combustion in industry
SC-IND-gas	Natural gas combustion in industry
PISP	Pig iron and primary steel production
NFMP-Cu	Copper primary production
NFMP-Pb	Lead primary production
NFMP-Zn	Zinc primary production
NFMP-Al	Aluminium primary production
NFMP-Au	Large-scale gold production
NFMP-Hg	Mercury production from mining
CEM	Cement production
OR	Oil refining
Intentional use and product waste associated sectors	
ASGM	Artisanal and small-scale gold mining
CSP	Chlor-alkali industry
WI	Incineration of product waste in large incinerators
WASOTH	Other disposal of product waste
CREM	Cremation emissions

Table B-6. Deposition from different emission sectors as simulated by GLEMOS, tonnes/year

	Area, km²	Stationary combustion sources	Industrial sources	Intentional use and product waste
NAM	1.69×10^{7}	24.1	20.0	25.0
EUR	5.53×10^{6}	22.8	12.6	12.7
SAS	5.07×10^{6}	29.3	18.7	14.2
EAS	1.16×10^{7}	52.0	54.2	21.9
SEA	4.94×10^{6}	6.9	13.4	14.0
PAN	8.06×10^{6}	3.5	8.5	11.2
AFR	3.00×10^{7}	28.0	39.8	57.4
MDE	5.17×10^{6}	2.6	6.3	7.4
MCA	5.21×10^{6}	4.0	10.8	15.6
SAM	1.53×10^{7}	7.3	25.1	37.4
CIS	1.79×10^{7}	19.6	29.1	28.0
ARC	2.24×10^{7}	8.2	19.7	22.6
ANT	3.42×10^{7}	9.1	23.3	40.3

Table B-7. Deposition from different emission sectors as simulated by GEOS-Chem, tonnes/year

	Area, km²	Stationary combustion sources	Industrial sources	Intentional use and product waste
NAM	1.69×10^{7}	32.4	34.8	41.1
EUR	5.53×10^{6}	22.3	15.6	15.3
SAS	5.07×10^{6}	27.7	21.2	17.9
EAS	1.16×10^{7}	56.9	71.6	42.0
SEA	4.94×10^{6}	7.9	14.1	16.4
PAN	8.06×10^{6}	4.7	11.1	16.4
AFR	3.00×10^{7}	33.7	50.0	80.7
MDE	5.17×10^{6}	3.7	8.3	10.2
MCA	5.21×10^{6}	5.2	13.2	22.3
SAM	1.53×10^{7}	11.3	34.1	58.6
CIS	1.79×10^{7}	27.3	42.9	40.4
ARC	2.24×10^{7}	9.0	19.8	20.3
ANT	3.42×10^{7}	8.0	19.1	34.2

Table B-8. Deposition from different emission sectors as simulated by GMHG, tonnes/year

		Stationary combustion sources	Industrial sources	Intentional use and product waste
NAM	1.69×10^{7}	22.9	33.9	36.4
EUR	5.53×10^{6}	11.4	12.8	12.7
SAS	5.07×10^{6}	13.0	15.0	14.8
EAS	1.16×10^{7}	26.2	40.3	34.0
SEA	4.94×10^{6}	7.4	13.6	18.4
PAN	8.06×10^{6}	6.3	11.8	17.4
AFR	3.00×10^{7}	34.4	55.5	86.9
MDE	5.17×10^{6}	5.4	9.5	11.1
MCA	5.21×10^{6}	5.7	10.9	17.7
SAM	1.53×10^{7}	13.0	26.0	47.0
CIS	1.79×10^{7}	21.4	35.1	33.6
ARC	2.24×10^{7}	17.6	31.5	30.6
ANT	3.42×10^{7}	9.2	16.3	26.3

a) GLEMOS

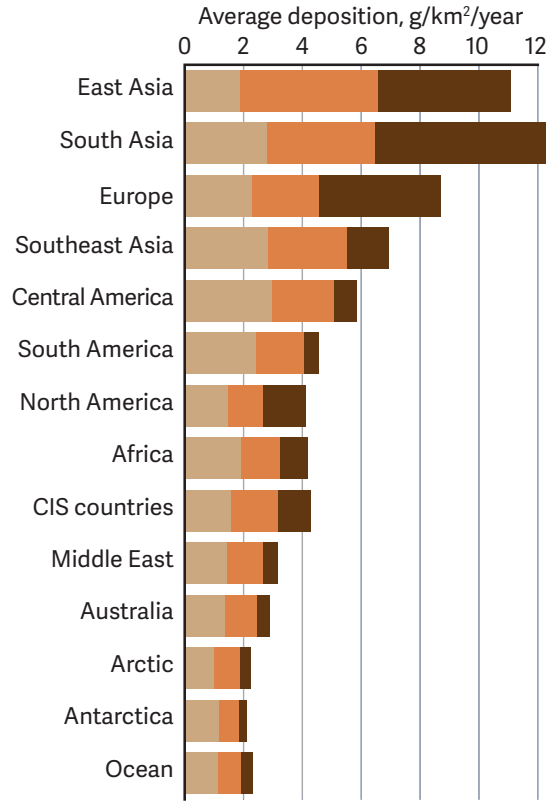

c) GMHG

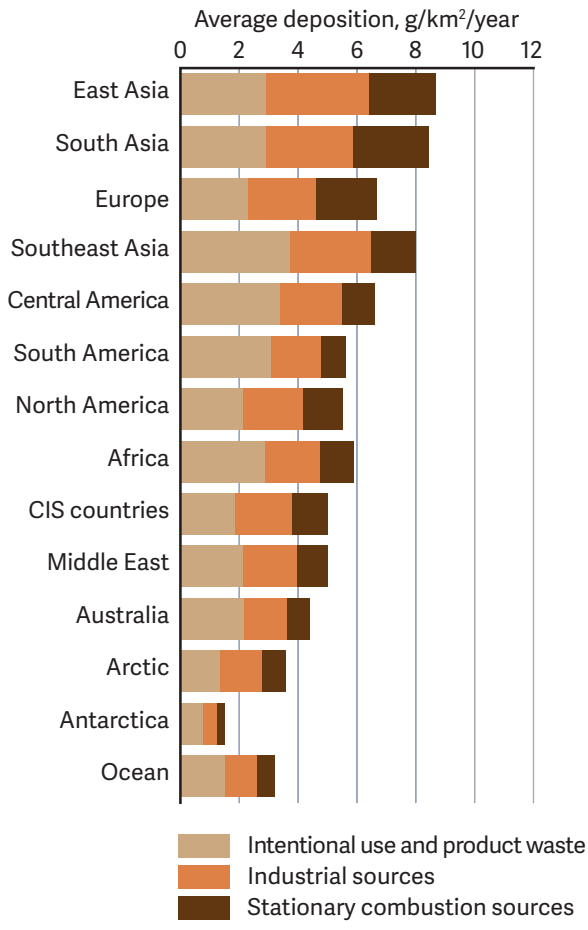

b) GEOS-Chem

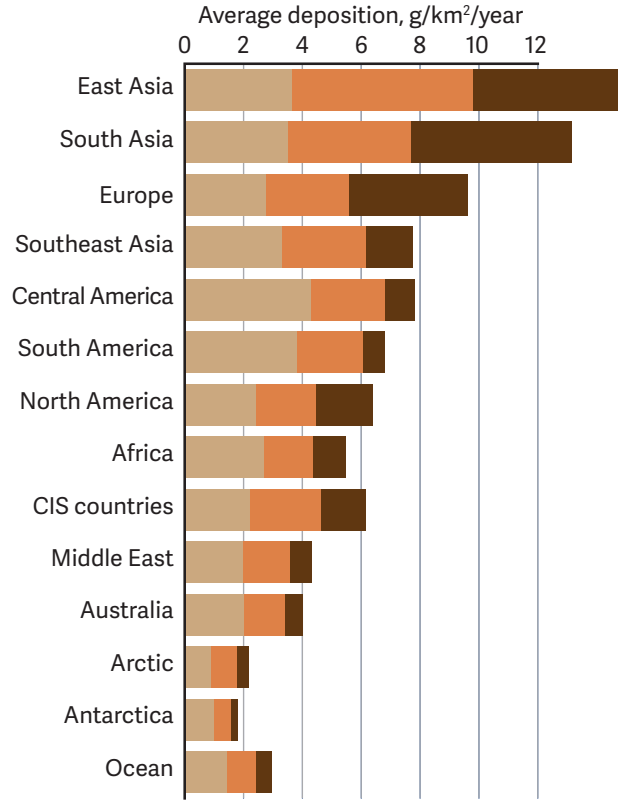

Figure B-8. Contribution of emissions from the three sector-specific groups to average mercury deposition from contemporary anthropogenic sources over various geographical regions in 2013.

UNEP
Division of Technology, Industry and Economics (DTIE)
Chemicals Branch
Geneva
Switzerland
May, 2015

Job Number: DTI/1905/GE

www.unep.org

United Nations Environment Programme
P.O. Box 30552 Nairobi, Kenya
Tel: ++254-(0)20-762 1234
Fax: ++254-(0)20-762 3927
E-mail: uneppub@unep.org

UNEP

AMAP Secretariat
Gaustadalléen 21
N-0349 Oslo
Norway
Tel. +47 21 08 04 80
Fax +47 21 08 04 85
amap@amap.no
http://amap.no

ISBN: 978-82-7971-087-5

AMAP
Arctic Monitoring and Assessment Programme